

Superoutbursts and Positive Superhumps are Detected During the Standstill in AT Cnc

Qi-Bin Sun^{1,2}, Sheng-Bang Qian^{1,2*}, Li-Ying Zhu^{3,5}, Qin-Mei Li⁴, Fu-Xing Li^{3,5}, Min-Yu Li^{3,5}, and Ping Li^{3,5}

¹Department of Astronomy, School of Physics and Astronomy, Yunnan University, Kunming 650091, China

²Key Laboratory of Astroparticle Physics of Yunnan Province, Yunnan University, Kunming 650091, China

³Yunnan Observatories, Chinese Academy of Sciences, Kunming 650216, China

⁴Guizhou University, Department of Physics, college of physics, Guizhou university, Guiyang, 550025, China

⁵University of Chinese Academy of Sciences, No.19(A) Yuquan Road, Shijingshan District, Beijing, China

*e-mail: qiansb@ynu.edu.cn

ABSTRACT

The disk instability model suggests that the disk remains in a hot state during standstill. The thermal-tidal instability model posits that superoutbursts require a mass ratio of $q = M_2/M_1 \leq 0.25 - 0.33$. However, this paper presents evidence of superoutbursts and positive superhumps (PSHs) during a standstill of AT Cnc ($q > 0.33$), based on both space- and ground-based photometric data from sky surveys. Notably, the PSHs evolve gradually prior to the onset of a superoutburst, suggesting that an eccentric, prograde-precessing disk forms first, with the superoutburst occurring as the radius of the accretion disk continues to expand. These observations indicate that, during the standstill, the disk radius in AT Cnc not only surpasses the tidal truncation radius and the 3:1 resonance radius, but is still undergoing expansion. Our analysis further reveals that superoutbursts are triggered by oscillations, which appear to be a characteristic feature of special dwarf nova outbursts. Additionally, we observe that special outbursts develop from normal outbursts, implying that certain stages of the disk may not reach a fully hot state during the standstill. Furthermore, the PSH amplitude was found to be correlated with special outbursts, revealing that the localized thermal instability had a significant impact on the evolution of the eccentric disk. These findings provide the first detailed observational evidence of superoutbursts and PSHs occurring during standstill, offering important new insights into the classification of dwarf novae and the underlying mechanisms of outbursts.

keywords: Binary stars; Cataclysmic variable stars; Dwarf novae; Z Camelopardalis; SU Ursae Majoris; individual (AT Cnc)

1 Introduction

Dwarf novae (DNe) are a significant subclass of cataclysmic variable stars (CVs) that have been a focus of extensive astronomical research, distinguished by their intermittent outbursts (Warner, 1995). In competition with various other models, the thermal-viscous instability model (DIM) in accretion disks has been widely used to explain the DN outbursts (e.g., Bath et al., 1974; Lasota, 2001; Lin et al., 1985; Meyer and Meyer-Hofmeister, 1983; Mineshige and Osaki, 1983; Osaki, 1974; Smak, 1983). A key process in this mechanism to explain intermittent outbursts is the viscous process caused by the magnetorotational instability (MRI, Balbus and Hawley, 1991), which plays a crucial role in angular momentum transfer and mass transport within the disk. During the quiescence, the accretion disk is in a low-temperature, low-viscosity state. As mass accumulates in the disk, its temperature rises to about 8000 K, leading to partial ionization of hydrogen. The opacity of the hydrogen is sensitive to changes in temperature, which triggers the instability of the disk, which transitions to a high-temperature, high-viscosity state when the hydrogen is fully ionized (see e.g., Lasota, 2001; Dubus et al., 2018; Hameury, 2020 for details).

The three main subtypes of DNe are U Geminorum (U Gem), Z Camelopardalis (Z Cam), and SU Ursae Majoris (SU UMa) (Warner, 1995). U Gem is the prototype of DNe. Systems of this type typically experience outbursts of 2-5 magnitudes, lasting for approximately 1-2 weeks, with a recurrence time of about a few months. U Gem stars are characterized by the standard behavior seen in classical DNe. Z Cam are notably characterized by a "standstill" during the decline of an outburst, where the brightness stabilizes approximately 0.7 mag below the peak. This phenomenon is explained by the combination of DIM and mass transfer fluctuations. For typical Z Cam stars, the mass transfer rate from the secondary star is usually close to a critical value (\dot{M}_{crit}). Small variations in this rate can trigger the standstill, which corresponds to the hot branch in the DIM (Meyer and Meyer-Hofmeister, 1983; Smak, 1983). Eventually, the standstill ends with a return to the quiescence. However, during the "Z CamPaign" observation campaign, Simonsen (2011) discovered an intriguing anomaly in some systems, such as IW

And and V513 Cas, where the standstill did not conclude with a return to quiescence. Instead, these systems experienced an outburst at the end of the standstill. Several other objects exhibiting similar behavior have been identified, such as ST Cha (Kato and Kojiguchi, 2021), IM Eri (Kato et al., 2020), KIC 9406652 (Kimura et al., 2020a) and Karachurin 12 (Sun et al., 2024d). These stars are classified as "IW And-type objects" (Kato, 2019), presenting a new challenge for the DIM. The fact that accretion disks, already in hot, high-viscosity state, can still undergo outbursts challenges the traditional understanding of the disk's behavior in the DIM.

The most distinctive feature of SU UMa-type DNe is the occurrence of superoutbursts, which are typically 0.5–1 mag brighter than normal outbursts and can last five to ten times longer. These superoutbursts are accompanied by positive superhumps (PSHs), typically a few percent longer than the orbital period. Understanding the mechanisms behind superoutbursts and PSHs has been a key component in the development of models for DN outbursts (Howell et al., 1995; Marino and Walker, 1974; Osaki, 1985; Papaloizou and Pringle, 1979; Vogt, 1974, 1982; Warner, 1985; Whitehurst, 1988; Whitehurst and King, 1991). The thermal-tidal instability (TTI), proposed by Osaki (1989), has become the commonly explanation for the phenomenon. TTI builds upon the framework of the DIM, assuming that mass transfer from the secondary star remains stable. According to TTI, all outburst activity is driven by instabilities within the accretion disk. During a normal outburst, the radius of the accretion disk expands until it exceeds the critical radius for the 3:1 resonance. Once this occurs, the system experiences a tidal instability, resulting in an eccentric disk with a slow prograde precession. The tidal torque exerted on the eccentric disk significantly amplifies the energy released during the outburst, leading to a superoutburst. Additionally, the outer regions of the eccentric disk are periodically subjected to tidal stresses from the secondary star, giving rise to the periodic PSHs (Osaki, 1985; Vogt, 1982; Wood et al., 2011).

It is worth noting that there are two types of precessing disks in CVs, the eccentric prograde precessing disk and the tilted disk retrograde precessing disk. The retrograde precession of tilted accretion disk induces a superorbital signal. In addition, the streams from the secondary interacting with the tilted disk produces "negative superhumps" (NSHs) that are a few percent shorter than the orbital period (e.g., Barrett et al., 1988; Harvey et al., 1995; Katz, 1973; Wood et al., 2009). Our recent study provides some evidence for the existence of tilted disks and the origin of NSHs (Sun et al., 2023c, 2024c, 2023b, 2024b).

AT Cnc is a classic Z Cam-type DN, and since its discovery by Romano and Persinotto (1968), multiple outbursts and standstills have been observed (Bond and Tifft, 1974; Gotz, 1983, 1987; Götz, 1991; Kato et al., 2001; Nogami et al., 1999). For a comprehensive history of research on this system, see Nogami et al. (1999), Kozhevnikov (2004), and Bruch et al. (2019) for detail. Notably, the orbital period of AT Cnc was first determined to 0.2011(6) days (4.83(1) hours) from spectroscopic observations by Nogami et al. (1999). Kozhevnikov (2004) observed signals with periods of approximately 4.65–4.74 hours and 1700–1800 seconds during the standstill, which they interpreted as likely corresponding to NSHs and quasi-periodic oscillations. However, Bruch et al. (2019), based on more recent photometric observations, did not detect any NSHs and updated the orbital period to 0.201634(5) days. Additionally, they identified a signal with a period of approximately 25.731(5) minutes (~ 1500 s). Boneva et al. (2024) also reported detecting oscillations with periods of around 20–30 minutes. Furthermore, a significant discovery was made by Shara et al. (2012), who detected a classical nova shell around the system, believed to be the remnant of a nova eruption that occurred ~ 330 years ago (Shara et al., 2017).

This paper investigates the standstill, outbursts, and PSHs of AT Cnc based on data from the Space Survey (Transiting Exoplanet Survey Satellite, TESS), Ground-Based Survey (All-Sky Automated Survey for Supernovae, ASAS-SN; Zwicky Transient Facility, ZTF; Wide Angle Search for Planets, SuperWASP), and American Association of Variable Star Observers (AAVSO) (see Fig. A1). For a detailed description of the data, see Appendix. While recent studies have suggested the occurrence of superoutbursts in Z Cam systems Kato et al. (2019, 2021), detailed variations were not resolved due to limitations in data resolution. For the first time, we present evidence of superoutburst and PSH production during a standstill of AT Cnc.

2 Analysis and Results

2.1 Signals

TESS observed two short outbursts of AT Cnc (during Sector 21: S21), and two standstills (S44-S47 and S71-S72; see the top panel of Fig. A2). The orbital period of AT Cnc, determined by Nogami et al. (1999) to be 0.2011(6) days, from the $H\alpha$ radial velocity measurements. The orbital period was recently updated to 0.201634(5) days by Bruch et al. (2019) based on photometric observations. We performed a frequency analysis of the segments S21, S44-S47, and S71-S72 using the Period04 software (details in Lenz and Breger, 2005). In the S21 segment, the orbital signal is present at the fundamental frequency, with a weak signal at twice the orbital frequency (see the bottom panel of Fig. A2(a)). In the frequency spectra of the S44-S47, S71, and S72 segments, a stable orbital signal is detected (see the bottom panel of Fig. A2). The average orbital period is determined to be 0.201754(3) days ($4.9565(8) \text{ d}^{-1}$). A periodic variation with a period of 5.577(4) days ($0.1793(1) \text{ d}^{-1}$) is found in the S44-S47. A large amplitude variation with a period of 5.056(3) days ($0.1978(1) \text{ d}^{-1}$) is detected in S71, and will be further discussed in Section 2.2. Additionally, superoutbursts and PSHs are observed in S71-S72, which will be discussed in Section 2.3.

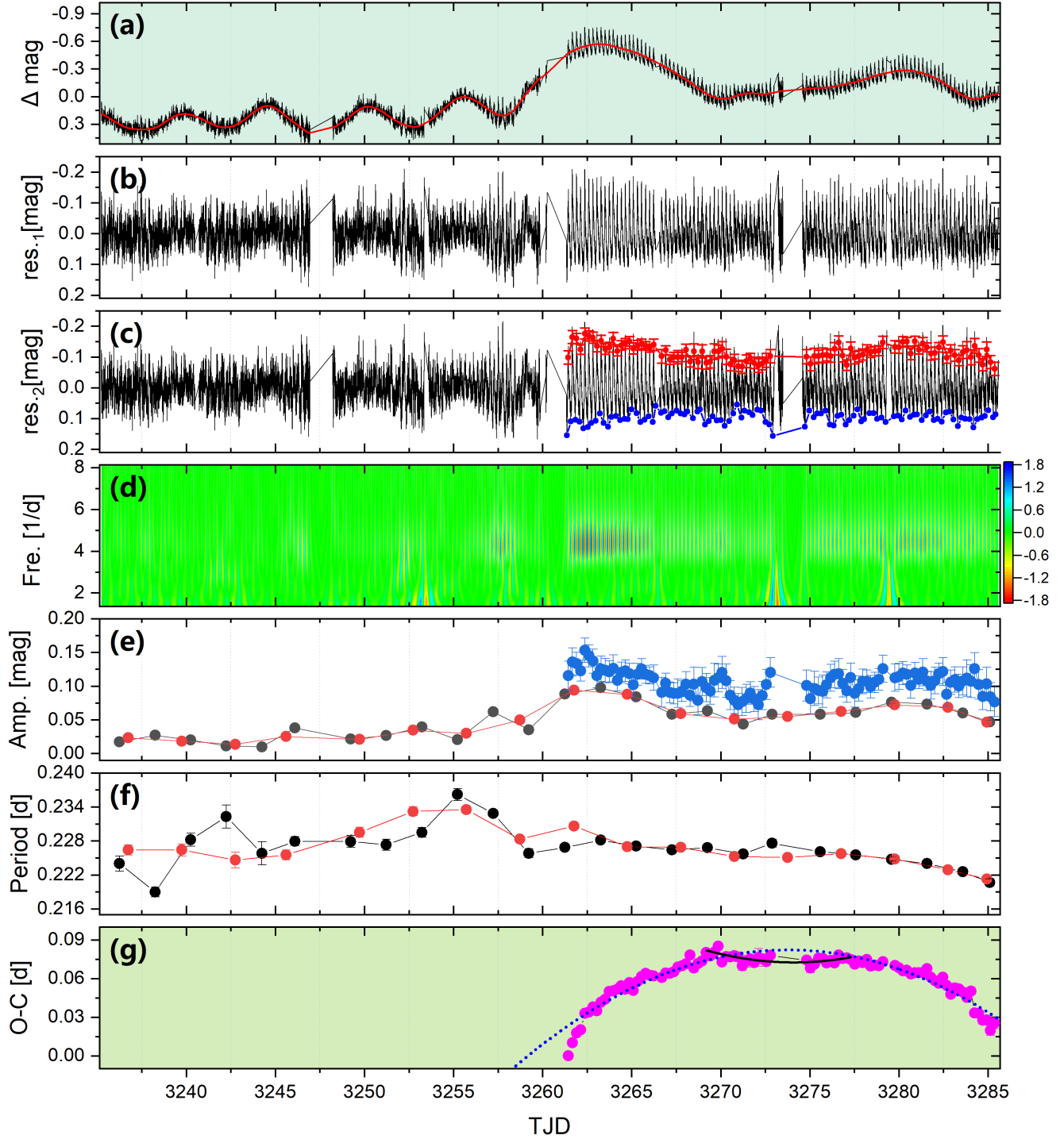


Figure 1. Results and process of analyzing PSHs in AT Cnc. (a) Light curves of S71-S72, the red solid line is the LOWESS fit; (b) LOWESS fit residuals (res_{-1}); (c) Light curve after removing the orbital signal (res_{-2}), the red dots are the maxima of the PSHs and the blue dots are the minima; (d) 2D power spectra of the CWT for res_{-2} , colors indicate the relative strength of the oscillations; (e) Black, red, and blue colors represent the amplitudes obtained by Fourier analysis of the 2-day segments, the 3-day segments, and the amplitudes obtained by the difference between the maxima and minima; (f) Black, red and blue represent the PSH periods obtained by Fourier analysis of 2-day segments and 3-day segments; (g) O-C analysis of the maxima of the PSHs, the blue dotted line and the black solid line are parabolic fits to all all O-C values and Stage B, respectively.

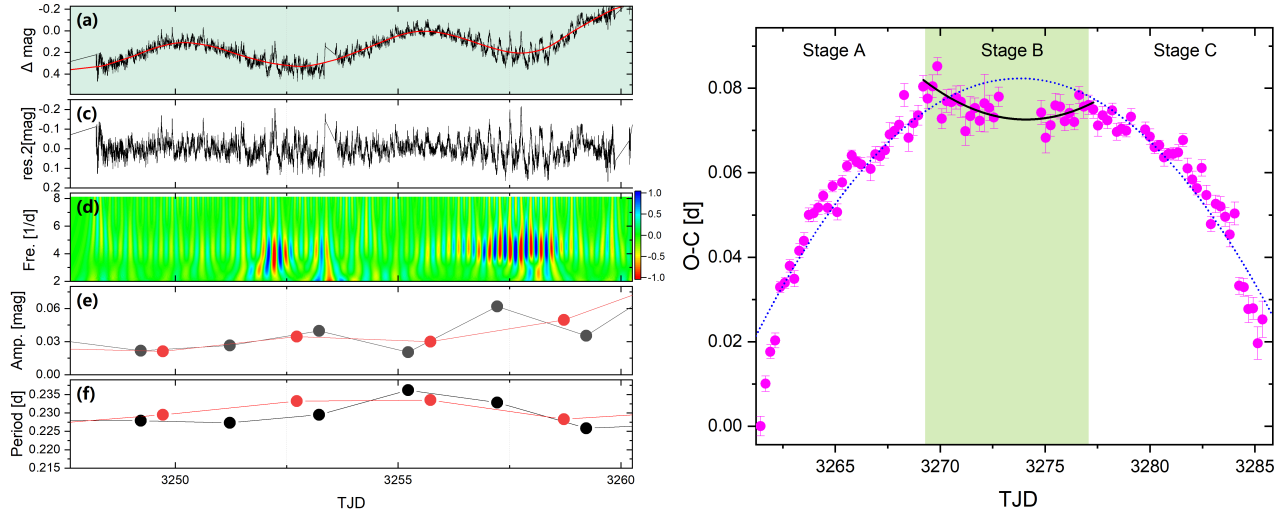


Figure 2. Left Panel: A magnified view of the changes in PSHs within S71, with individual panels mirroring the presentation style of Fig. 1. Right Panel: The O-C plot of the maxima of PSHs in S72, which is consistent with the data representation of Fig. 1(g).

2.2 Standstills and Outbursts

In our study, we observed that the S44-S47 and S71 exhibited periodic variations with periods of $P_{S44-S47} = 5.577(4)$ days ($Amp_{S44-S47} \sim 0.03$ mag) and $P_{S71} = 5.056(3)$ days ($Amp_{S71} \sim 0.11$ mag), respectively. This oscillation period is shorter than the outburst cycle ($8.13(\pm 2.68)$ days to $14.49(\pm 3.34)$ days, see Section 4). We further investigated whether similar periodic phenomena were present during other standstills. In two specific time intervals, JD2457742.3908 to JD2457792.4472 (see Figs. 3(b) and (e)) and JD2458152.8375 to JD2458213.9356 (see Figs. 3(c) and (f)), we indeed observed significant oscillations, with sine-fit periods of 6.43(5) days and 8.08(1) days, respectively. This implies that this oscillation is not an isolated case.

Considering that no NSHs were detected in the spectra corresponding to S44-S47 and S71, we can exclude the possibility of tilted disk precession. Based on the PSH and the orbital period, the predicted eccentric disk precession period is ~ 1.82 days ($1/P_{\text{prec}} = 1/P_{\text{orb}} - 1/P_{\text{psh}}$), which is shorter than the observed oscillation periods. Therefore, we can conclude that the possibility of luminosity fluctuations caused by prograde precession of an eccentric disk.

Particularly, between JD2457425.5479 and JD2457536.8826, the light curve of AT Cnc revealed an interesting phenomenon: after a brightness drop of about 0.7 mag following an outburst, a standstill period of approximately 15 days followed. At the end of this standstill, AT Cnc attempted to return to a quiescence but failed to fully stabilize, and a new outburst cycle began (see Fig. 3(g)). This new outburst lasted about 8 days before entering a phase of repetitive oscillations, with amplitude and period gradually decreasing until reaching a minimum, then gradually increasing again, eventually evolving into a typical outburst pattern. The shortest oscillation interval was about 5 days, similar to the oscillations observed in S44-S47 and S71.

Therefore, we infer that the oscillations observed in S44-S47 and S71 are likely to be special DN outbursts, which evolve from normal outbursts, decreasing in period and amplitude with a gradual rise to a stagnation, and resuming again as normal outbursts with the end of the standstill.

2.3 Superoutbursts and Positive Superhumps

The oscillations in S71 was an overall increasing trend, which eventually triggered the superoutburst. This further confirms that this oscillation is a special DN outburst. The superoutburst is about 0.7 mag brighter than the special outburst, lasts at least about 30 days, and there are significant PSHs during the superoutburst (see Fig. 1), all of which are similar to the SU UMa-type DNe. The presence of PSHs is detected in both the S71 and S72 sectors. This section will provide a detailed analysis of the PSHs. To present the generation and evolution of PSHs in detail, we adopted the analysis method of Sun et al. (2024a) and Sun et al. (2024d), and followed the steps outlined below:

- (i) The locally-weighted polynomial regression (LOWESS; Cleveland, 1979) fit with a 2-day span was applied to remove the long-term trends, and the results are shown in Figure 1(a) and (b).
- (ii) Frequency analysis of the residuals (residual_1) from the LOWESS fit was performed using the Period04 to obtain the parameters for the orbital signal and its second harmonic. The orbital signal was then removed to eliminate the interference in the PSH calculation using the following formula (see Tab. A6):

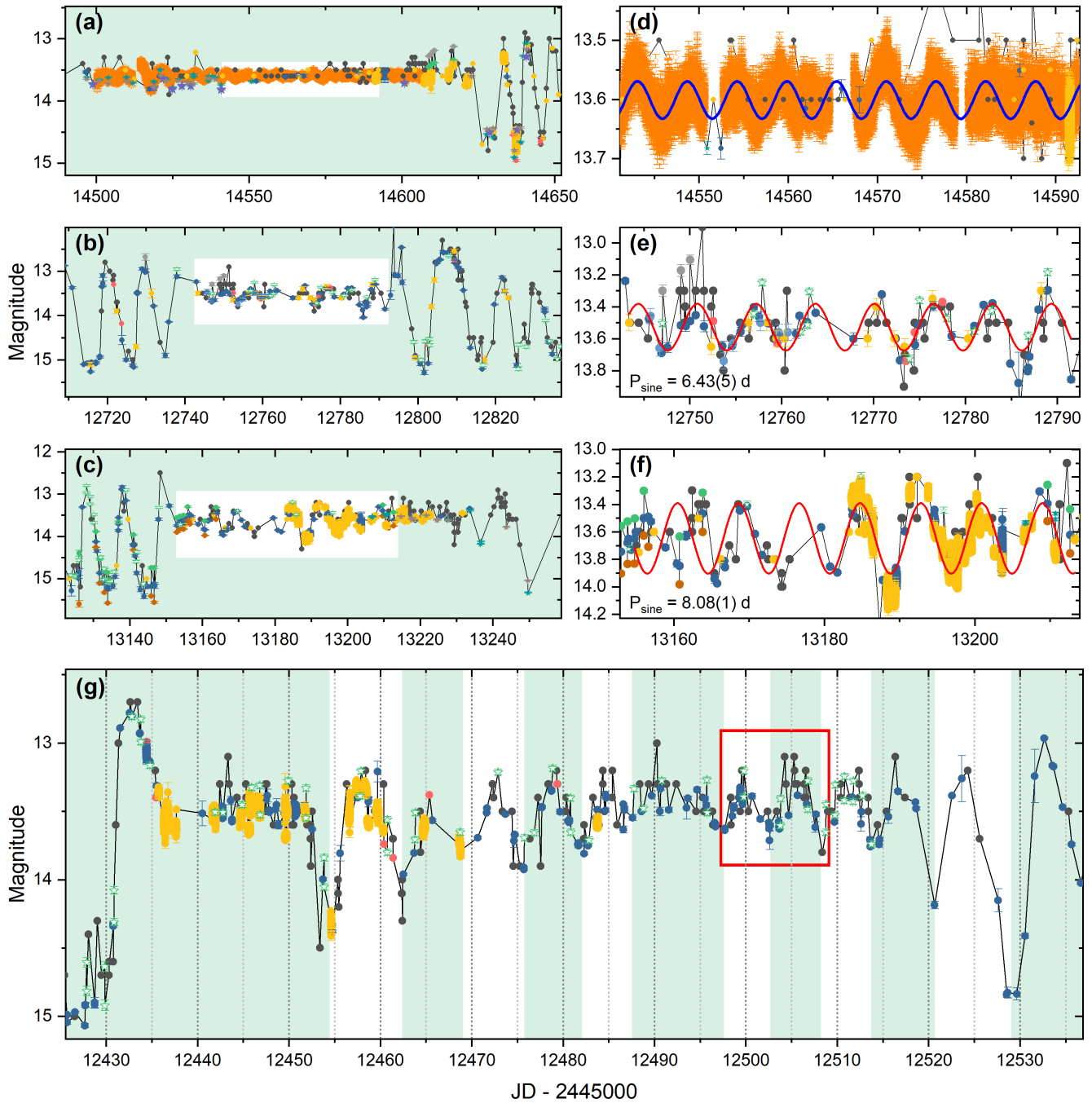


Figure 3. Oscillations during the brightness standstill of AT Cnc Panels (a), (b), and (c) display three light curves showing brightness standstill with oscillations. Panels (d), (e), and (f) provide magnified views of the white rectangular regions from panels (a), (b), and (c), respectively, with sine fits overlaid on the curves. Panel (g) illustrates the oscillation generation process, with the red rectangular box highlighting the two shortest oscillation intervals, approximately 5 days.

$$LC_{\text{orb}}(t) = Z + \sum \text{Amplitude}_i \cdot \sin(2\pi \cdot (\text{frequency}_i \cdot t + \text{phase}_i)) \quad (1)$$

where Z , Amplitude_i , frequency_i , and phase_i are the fitted intercept, amplitude, frequency, and phase, respectively. The residual₂ after the orbital signal removal is given by: $\text{residual}_2 = \text{residual}_1 - LC_{\text{orb}}$. The frequency spectra of residual₁ and residual₂ are shown as black and red lines in the right panel Figure A2(e).

- (iii) A segmented frequency analysis was conducted on residual₂ with segment intervals of 2 days and 3 days. The results are shown in Figure A4 and Table A6.
- (iv) The Continuous Wavelet Transform (CWT; Polikar et al., 1996) was applied to residual₂ as a cross-validation of the segmented frequency analysis. The results are presented in Figure 1(d).
- (v) The significant PSHs in S72 provided an opportunity to determine the parameters of each PSH. We used a linear superposition of Gaussian fits to calculate the peak information of the PSHs (see Fig. 1(c)). Based on the fit, the first maxima and the average PSH period from the segmented (3d) analysis of S72, we derived the following epoch:

$$\text{Maxima} = \text{TJD}3261.4371(23) + E \times 0.22551(33) \text{d} \quad (2)$$

Using this epoch formula, an O-C (observed minus calculated) analysis of the PSHs was performed, and the results are shown in Figure 1(g).

- (vi) A parabolic fit was applied to the O-C curve obtained from step (v). The results are shown in Figure 2. The O-C curve of AT Cnc suggests a possible Stage B similar to other SU UMa-type DNe. A separate parabolic fit for the Stage B is shown in the black curve in Figure 2.
- (vii) Based on the maxima obtained in step (v) and the two minima before and after the PSH peak, we calculated the half-amplitude of each PSH using the following formula, which serves as a complementary result to the segmented frequency analysis and CWT:

$$\Delta \text{Amplitude}_{\text{psh}} = \frac{(\text{minima}_{\text{before, mag}} + \text{minima}_{\text{after, mag}}) / 2 - \text{maxima}_{\text{mag}}}{2} \quad (3)$$

Here, $\text{minima}_{\text{before, mag}}$ and $\text{minima}_{\text{after, mag}}$ refer to the magnitudes of the minima before and after the PSH maxima, respectively.

Based on the analysis outlined above, we draw the following conclusions:

- (a) In step (V), regardless of whether frequency analysis is performed by dividing the data into two-day or three-day segments, PSHs consistently emerge (see Fig. A4). By averaging the results of frequency analysis using three-day segments, we obtain the average period and amplitude of the PSHs as 0.22689(59) days and 0.048(1) mag, respectively. The ϵ is determined to be 0.1246(31) ($\epsilon = (P_{\text{psh}} - P_{\text{orb}}) / P_{\text{orb}}$). By comparing the analysis results at segmented frequency analysis, wavelet transforms, and the amplitudes determined between the maxima and minima, we observe that the PSH amplitude begins to increase at the S71, reaches its peak at the S72 superoutburst, and then remains at a higher amplitude level thereafter (see Fig. 1).
- (c) A comparative analysis of the residuals (residual₂) of the light curve during the S71, segmental fourier transform results, and CWT reveals that PSHs do not arise in a linear fashion. As the overall brightness increases, the amplitude of the PSHs exhibits an oscillatory growth pattern, with amplitude changes associated with a signal that has a period of $P_{S71} = 5.056(3)$ days (special DN outbursts). Specifically, the PSH amplitude gradually increases when the special DN outbursts weaken, and decreases accordingly when the outbursts increase (see Figs. 1 and 2).
- (b) The results of the segmental analysis reveal that the PSH period slowly increases during the S71, and then gradually decreases after the initiation of the superoutburst. This trend is corroborated by the O-C analysis. A parabolic fit to the entire O-C dataset shows that the rate of change of the PSH period during the superoutburst is $\dot{P} = -1.74(\pm 0.07) \times 10^{-4}$ days/day. According to Kato et al. (2015); Kato et al. (2009, 2012), the evolution of the PSH period in SU UMa-type

DNe is divided into three distinct stages: Stage A, Stage B, and Stage C. In Stage A, which marks the early evolutionary phase, the superhump period is the longest, with no noticeable change in the period. In Stage B, the period starts to vary, showing a positive period derivative. Finally, Stage C is characterized by a shorter, more stable superhump period. AT Cnc was similarly found to be present in stage B, but the PSH period remained consistently decrease in stage A and C (see Figs. 1(g) and 2). The parabolic fit for the Stage B yields a period change rate of $\dot{P} = +1.77(\pm 0.84) \times 10^{-4}$ days/day.

3 DISCUSSION

3.1 Special dwarf nova outbursts

The standstill phenomenon in Z Cam systems has typically been attributed to the combination of the DIM and fluctuations in mass transfer. Several statistical results and simulations have supported the plausibility of this widely accepted explanation (Dubus et al., 2018; Hameury, 2020; Honeycutt et al., 1998; Meyer and Meyer-Hofmeister, 1983; Smak, 1983). However, the discovery of IW And objects challenges this model (Kato, 2019; Simonsen, 2011). According to DIM, the accretion disk during the standstill phase of Z Cam systems is expected to already be in a hot state, which should transition into a quiescent phase. In contrast, IW And systems often exhibit an outburst after standstill, deviating from this expected behavior. One hypothesis suggests that accretion disk instability, driven by secondary mass-transfer outbursts, could explain this phenomenon (Hameury and Lasota, 2014), though the origin of these outbursts remains unclear. Alternatively, a tilted-thermal instability model (tilted-DIM) proposes that a tilted disk may maintain a hot state by allowing mass to flow directly into the inner disk (Kimura et al., 2020b). However, simulations based on the tilted-DIM have encountered difficulties in reproducing the details of the IW And phenomenon (Kimura et al., 2020b; Sun et al., 2024d).

In this study, we analyze TESS data and identify distinct long-period oscillations during the standstill phase of AT Cnc. We observe that normal outbursts evolve into these oscillations, which transition back to normal outbursts as the standstill phase ends (see Fig. 3(g)). Furthermore, the amplitude of the oscillations in S71 gradually increases, eventually triggering a superoutburst (see Fig. 1), resembling the superoutbursts seen in SU UMa systems. This behavior suggests that these oscillations represent a special DN outburst. This finding implies that superoutbursts, as well as DN outbursts, can occur during the standstill, prompting a revision of the traditional DIM framework. Specifically, during some standstill phases of the Z Cam system, as suggested by the tilted-DIM, the disk may not be in a fully hot state, but rather a localized zone of high temperature may occur. The fact that AT Cnc did not detect the presence of a tilted disk suggests that this incomplete hot state condition may not have a direct correspondence with the tilted disk.

3.2 Eccentric disk precession

TTI proposes that the mass transfer from the secondary star is stable, with a continuous accumulation of mass onto the accretion disk during each normal outburst. The disk's radius gradually expands, eventually surpassing the 3:1 resonance radius. At this point, tidal instability induces an eccentric progression of the disk, leading to superoutbursts and the formation of PSHs (Osaki, 1989). However, the disk radius is not expected to expand indefinitely. Upon reaching the tidal truncation radius, a strong tidal torque acts to extract angular momentum from the disk, thereby halting further expansion (Paczynski, 1977; Wakamatsu et al., 2021). The model further predicts that binaries exhibiting this phenomenon are characterized by mass ratios lower than 0.25 (Osaki, 2005; Whitehurst, 1988), with extreme cases having mass ratios below 0.33 (Murray et al., 2000).

Bruch (2023) identified a significant number of PSHs using TESS data, in conjunction with statistical data from Patterson et al. (2005), to derive an empirical relationship between the orbital period and ϵ ($P_{\text{orb}} - \epsilon$). The ϵ value for AT Cnc was found to be consistent with this correlation (see the left panel of Fig. 4). Nogami et al. (1999) had previously determined the mass ratio of AT Cnc to be 0.511, but with uncertainties. Therefore, we re-estimated the mass ratio of AT Cnc to be 0.41, based on the empirical relationship obtained by Patterson et al. (2005) and their analysis of $\epsilon(q)$. Using a similar methodology to that of Hellier (2001), Osaki and Meyer (2003), and Kato et al. (2008), we plotted the relationship between the 3:1 resonance radius, the 2:1 resonance radius, and the tidal truncation radius (see the right panel of Fig. 4). In both the cases with mass ratios of 0.511 and 0.41, the 3:1 resonance radius exceeds the truncation radius.

SU UMa-type superoutbursts have been classified into various types, all of which are predicted to generate PSHs following the final normal outburst (Osaki, 2005; Osaki and Meyer, 2003). Observational data have confirmed the formation of PSHs after the superoutburst has reached a certain stage (Court et al., 2019; Kato, 2022; Wei and Shengbang, 2023). The PSHs of AT Cnc have been detected since the beginning of the S71, and a superoutburst was triggered approximately 22 days after the last special outburst. This timing suggests that the eccentric prograde precessing disk was formed before the onset of significant tidal dissipation, and that the accretion disk continued to expand past both the truncation radius and the 3:1 resonance radius. The disk reached a critical size before the superoutburst occurred. This means that there may be a critical radius outside of the 3:1 resonance radius of the AT Cnc that will trigger the superoutburst to occur.

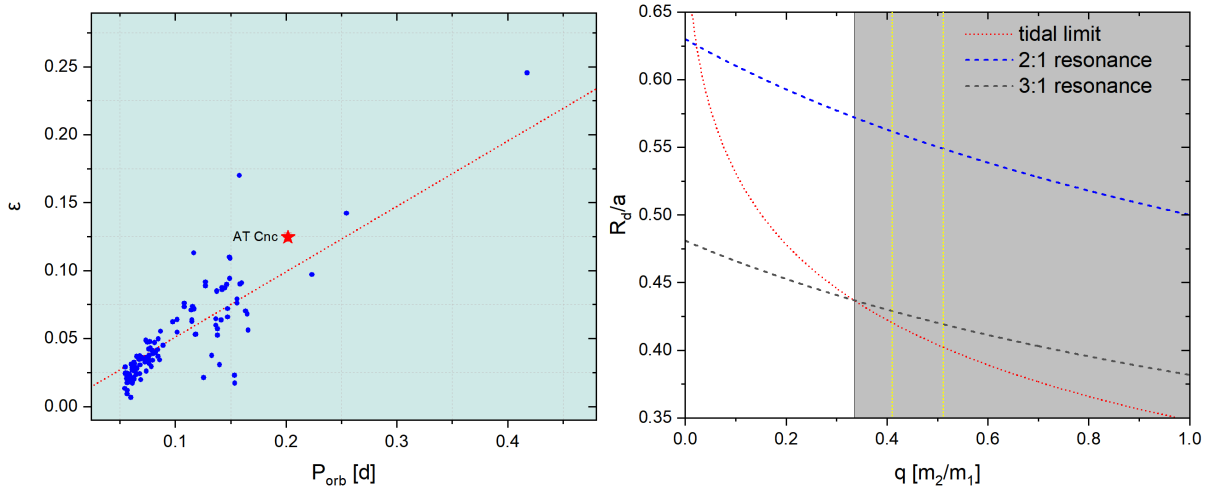


Figure 4. Left panel: blue dots from Bruch (2023) and Patterson et al. (2005), red dashed line is $P_{\text{orb}} - \epsilon$ relation from Bruch (2023), red pentagram corresponds to the position of AT Cnc. Right panel: black, blue and red dotted lines correspond to 3:1 resonance radius, 2:1 resonance radius and tidal truncation radius, vertical blue dashed lines correspond to $q=0.41$ and $q=0.511$.

3.3 Evolution of PSHs

In this paper, we find that the PSH amplitude oscillates and increases before the superoutburst occurs. The PSH amplitude gradually rises as the special outbursts wane, reaching a maximum at the bottom (see Figs. 1 and 2). The PSHs are thought to arise from the periodic tidal forces exerted by the secondary star on the eccentric disk, particularly on its protruding portion. In the TTI framework, the radius of the accretion disk oscillates and expands, with the disk growing during normal outbursts. During the decline of normal outbursts, the accretion disk contracts, limited by the low-angular-momentum mass influx from the secondary star. As a result, the disk radius at the peak of the special outbursts in AT Cnc is expected to be larger than at the minimum, corresponding to greater tidal pressures. However, this appears to be the opposite of the observed PSH amplitude changes.

If irradiation-induced mass transfer variations are taken into account, the secondary star is irradiated by the accretion disk during the outburst, which increases the mass transfer (Hameury, 2020; Knigge et al., 2000; Smak, 1995). This process would limit the expansion of the accretion disk. However, in the low state of the accretion disk, the disk continues to expand, a behavior that seems to correlate with the observed variation in the PSH amplitude of AT Cnc. While there remains some controversy surrounding irradiation-induced mass transfer variations, the changes in PSH amplitude can provide a useful window into understanding the underlying mechanism. Additionally, we suggest that the rate of eccentricity growth should also be considered (Lubow, 1991; Murray, 2000; Osaki, 2005). Within the TTI framework, if the rate of eccentricity growth exceeds the rate of contraction of the disk during the low state of the special outburst, leading to an extended protrusion of the eccentric disk, this could also explain the observed changes in PSH amplitude in AT Cnc. But the specific physical processes require a large number of calculations and simulations.

4 CONCLUSIONS

This paper investigates the Z Cam-type DN AT Cnc, located above the orbital gap, using data from TESS, ASAS-SN, SuperWASP, ZTF, and AAVSO. The main conclusions are as follows:

- (1) Based on the TESS data, the orbital period of AT Cnc was updated to 0.201754(3) days. PSHs were first detected with an average period of 0.22689(59) days and an eccentricity of $\epsilon = 0.1246(31)$.
- (2) Using TESS data, we identified long-period oscillations during AT Cnc's standstill. Specifically, in the S44-S47 sectors, the oscillation period was 5.577(4) days (amplitude ~ 0.03 mag), while in S71, the period was shorter, 5.056(3) days (amplitude ~ 0.03 mag). They can evolve from normal outbursts during standstill, later transitioning back into normal outbursts. Notably, the increasing amplitude of the oscillations in S71 triggered a superoutburst, similar to the behavior seen in SU UMa-type DNe. Therefore, these oscillations are classified as special DN outbursts, challenging the traditional DIM. This suggests that the accretion disk may alternate between localized hot regions and a fully hot state during some standstills.

- (3) The special outbursts in S71 show an upward trend and eventually trigger a superoutburst, indicating continued expansion of the accretion disk radius. This superoutburst was 0.7 magnitudes brighter than the special outburst and lasted at least 30 days, exhibiting characteristics typical of SU UMa-type DNe. In particular, it displayed behavior akin to Stage B in the O-C analysis. Analysis of the PSHs revealed that they had been present since S71 and lasted approximately 22 days before the superoutburst occurred. This suggests that the radius of the accretion disk continued to expand even after passing the 3:1 resonance radius.
- (4) Additionally, we found that the PSH amplitude was correlated with the phase of the special outburst, peaking in the low state, which is inconsistent with the prediction of the TTI. Irradiation-induced mass transfer variations and the rate of eccentricity growth may be potential factors influencing the PSH amplitude. However, extensive simulations and calculations are needed to further investigate these possibilities.

Acknowledgements

This work was supported by National Key R&D Program of China (grant No. 2022YFE0116800), the National Natural Science Foundation of China (Nos. 11933008). We would like to thank the teams and facilities behind the following surveys for providing the data used in this study: the All-Sky Automated Survey for Supernovae for their V-band data on AT Cnc, the Zwicky Transient Facility for their long-term monitoring of AT Cnc in multiple filters, the SuperWASP survey for their observations of AT Cnc over several years, the American Association of Variable Star Observers for their extensive collection of variable star data, and the Transiting Exoplanet Survey Satellite for providing high-quality space-based photometric data on AT Cnc. Their contributions have been invaluable to this research.

Appendix

A description of the data used in this paper and an estimate of the outburst periods, as well as some figures and tables, are included in the Appendix. **Figure A1:** Displays the light curves for all data sources. **Figure A2:** Light curves and corresponding frequency spectra of AT Cnc observed by TESS. **Table A3:** TESS photometric log for AT Cnc. **Figure A4:** Frequency spectra of segmented frequency analysis. **Figure A5:** Analysis of the AT Cnc outburst periods. **Table A6:** Frequency analysis results for different sectors and segments. **Table A7:** The outburst segments and the corresponding peak frequency parameters.

Data Sources and Outburst Period

The All-Sky Automated Survey for Supernovae (ASAS-SN; [Shappee et al., 2014](#), [Kochanek et al., 2017](#)) is a ground-based, automated survey project consisting of 24 small telescopes. It is dedicated to the rapid detection of supernovae across the entire sky, with a limiting magnitude of approximately $V \sim 17$. AT Cnc (ASAS-SN ID: ASASSN-V J082836.99+252002.8) was detected by ASAS-SN over a 5-year period in the V band, with an average magnitude of 13.92. Data were retrieved from the ASAS-SN Variable Stars Database ([Jayasinghe et al., 2019](#))¹.

The Zwicky Transient Facility (ZTF; [Bellm et al., 2019](#)) is an advanced automated optical time-domain survey using the Palomar 48-inch Schmidt Telescope, scanning the entire northern visible sky at approximately 3,760 square degrees per hour with a 47 square degree field of view and reaching median depths of $g \sim 20.8$ and $r \sim 20.6$ magnitudes (with a 30 s exposure; see [Masci et al. \(2019\)](#) and [Graham et al. \(2019\)](#) for detail). AT Cnc (ZTF ID: ZTF17aaagvsz) was monitored by the ZTF survey over approximately six years, from MJD 58206.2148 to MJD 60433.1983, using the ZTF filters ZTF_zg (mean magnitude 13.86), ZTF_zr (mean magnitude 13.90), and ZTF_zg (mean magnitude 13.86). The observational data were retrieved from the Lasair database².

The Wide Angle Search for Planets (SuperWASP) is a ground-based astronomical survey primarily aimed at discovering exoplanets. It consists of two robotic observatories: SuperWASP-North, located on La Palma, and SuperWASP-South in South Africa, ensuring continuous monitoring of both hemispheres. Each observatory houses eight wide-angle cameras with 11.1 cm apertures, providing a total field of view of almost 500 square degrees. Operating in a broadband filter range of 4000–7000 Å, it achieves photometric accuracy better than 1% for stars with magnitudes between 8 and 11.5. For more detailed information on the SuperWASP project, refer to [Pollacco et al. \(2006\)](#). AT Cnc (SuperWASP ID: 1SWASP J082836.92+252003.2) was recorded by four of the cameras (104, 141, 142, and 143) over a span of about 3.6 years, with an average magnitude of 13.84, downloaded from the DR1 of the WASP data ([Butters et al., 2010](#))³.

The American Association of Variable Star Observers (AAVSO; [Watson et al., 2006](#)) maintains a comprehensive record of observations for AT Cnc, collected through a global network of both amateur and professional astronomers. These observations

¹<https://asas-sn.osu.edu/variables>

²<https://lasair.roe.ac.uk/>

³<https://wasp.cerit-sc.cz/>

Table A3. TESS photometric log for AT Cnc.

Sectors	Start time [UT]	End time [UT]	Start time ^a [TJD]	End time ^a [TJD]
21	2020-01-21T22:33:32.974	2020-02-18T06:50:46.806	1870.44077	1897.78606
44	2021-10-12T16:51:01.448	2021-11-05T22:34:27.544	2500.20290	2524.44140
45	2021-11-07T05:26:38.228	2021-12-02T03:03:51.738	2525.72763	2550.62848
46	2021-12-03T12:05:58.954	2021-12-30T04:56:19.929	2552.00496	2578.70659
47	2021-12-31T07:40:23.644	2022-01-27T10:41:03.972	2579.82052	2606.94599
71	2023-10-17T17:49:07.811	2023-11-11T09:20:36.938	3235.24325	3259.89012
72	2023-11-11T16:24:39.674	2023-12-07T02:03:49.742	3260.18459	3285.58679

^a The units are BJD - 2457000.

span multiple methods and include data across nine photometric bands: Visual (Vis.), Unknown (N/A), Johnson V (V), Johnson B (B), Cousins R (R), Cousins I (I), Red Zeropoint (CR), Unfiltered with V Zeropoint (CV), and Tri-Color Green (TG). For a detailed description of these bands and their characteristics, please refer to the AAVSO documentation⁴. The AAVSO database contains a total of 74,874 data points collected over a period of 50 years, offering invaluable support for the in-depth study of AT Cnc. The data were downloaded from the AAVSO public database⁵.

The Transiting Exoplanet Survey Satellite (TESS; [Ricker et al., 2015](#)) is a space-based survey telescope launched by NASA in 2018. It is in a highly elliptical 13.7-day orbit around Earth, with the primary mission of detecting exoplanets via the transit method. TESS is equipped with four wide-field cameras, covering a total field of view of 24° by 96°, and operates in the 600–1000 nm wavelength range. TESS observes the sky by dividing it into sectors, each observed for about 27 days in two modes: long (30 min) and short (2 min). While TESS’s main goal is exoplanet discovery, it has also gathered extensive data on cataclysmic stars (CVs), making significant contributions to their study. We have conducted long-term research on CVs using TESS data (e.g., [Sun et al., 2023a](#); [Sun et al., 2023c](#); [Sun et al., 2024b](#); [Sun et al., 2024c](#)). AT Cnc (TESS ID: TIC 3645653) was observed in TESS sectors S21, S44–S47, and S71–S72 (see [Table A3](#)).

TESS data are managed by the Mikulski Archive for Space Telescopes (MAST), which provides two light curves: Simple Aperture Photometry (SAP) and Pre-search Data Conditioning Simple Aperture Photometry (PDCSAP). PDCSAP improves SAP by correcting sector discontinuities and removing systematic errors and anomalies (see [Jenkins et al., 2016](#); [Kinemuchi et al., 2012](#); [Twicken et al., 2010](#) for details). However, PDCSAP can occasionally distort dwarf nova outburst light curves ([Sun et al., 2024d](#); [Sun et al., 2024a](#)). Therefore, in this study, we used PDCSAP data for all sectors except S71–S72, where SAP data were used. The TESS data were downloaded from MAST⁶.

Since a single data source was insufficient to provide enough information to independently analyze these periods, we integrated all available data sources to calculate the outburst periods and selected observation gaps as natural breakpoints for segmented Fourier transform analysis. This process started from JD2449361.6940, as data prior to this date were relatively sparse. In the end, we divided the entire outburst process into 21 segments and selected peaks in the frequency range of 0 to 0.5 to determine the outburst period for each segment (see [Fig. A5\(a\)](#)). According to these analyses, we found that the range of outburst periods varied from 8.13 (± 2.68) days to 14.49 (± 3.34) days (see [Table A7](#) and [Fig. A5\(c\)](#)), with an average outburst period of about 11.67 (± 3.02) days. To validate these results, we performed a sine fit for the outburst segments with the shortest and longest periods, yielding fitting periods of 7.93 (± 1) days and 14.38 (± 3) days, respectively, which were consistent with the results of the frequency analysis (see [Fig. A5\(b\)](#)).

⁴<https://dev-mintaka.aavso.org/bands-optical-data-aavso-international-database>

⁵<https://www.aavso.org/LCGv2/>

⁶<https://mast.stsci.edu/>

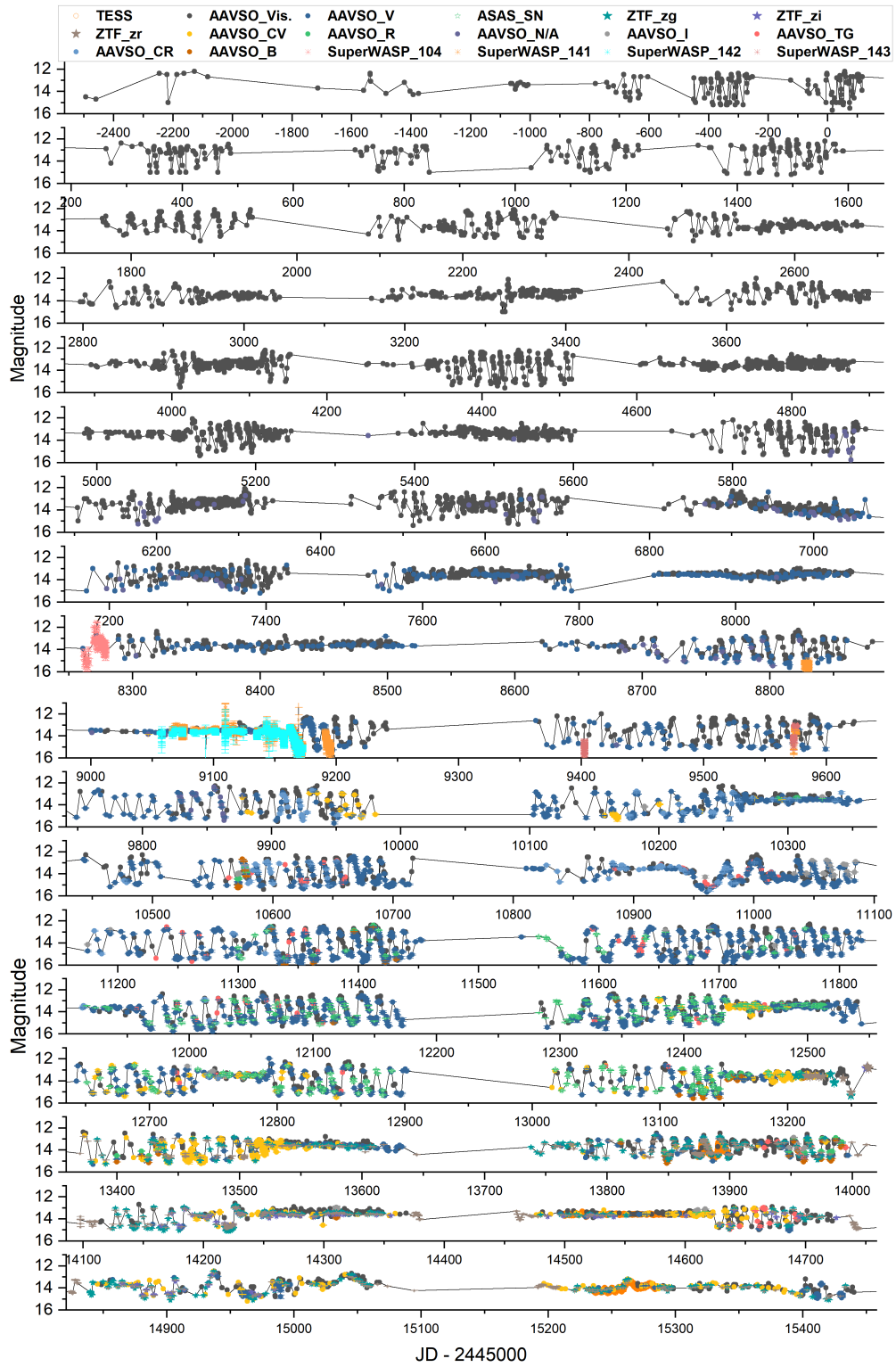


Figure A1. AT Cnc light curves for different data sources, refer to the figure legend for the meaning of the different symbol codes.

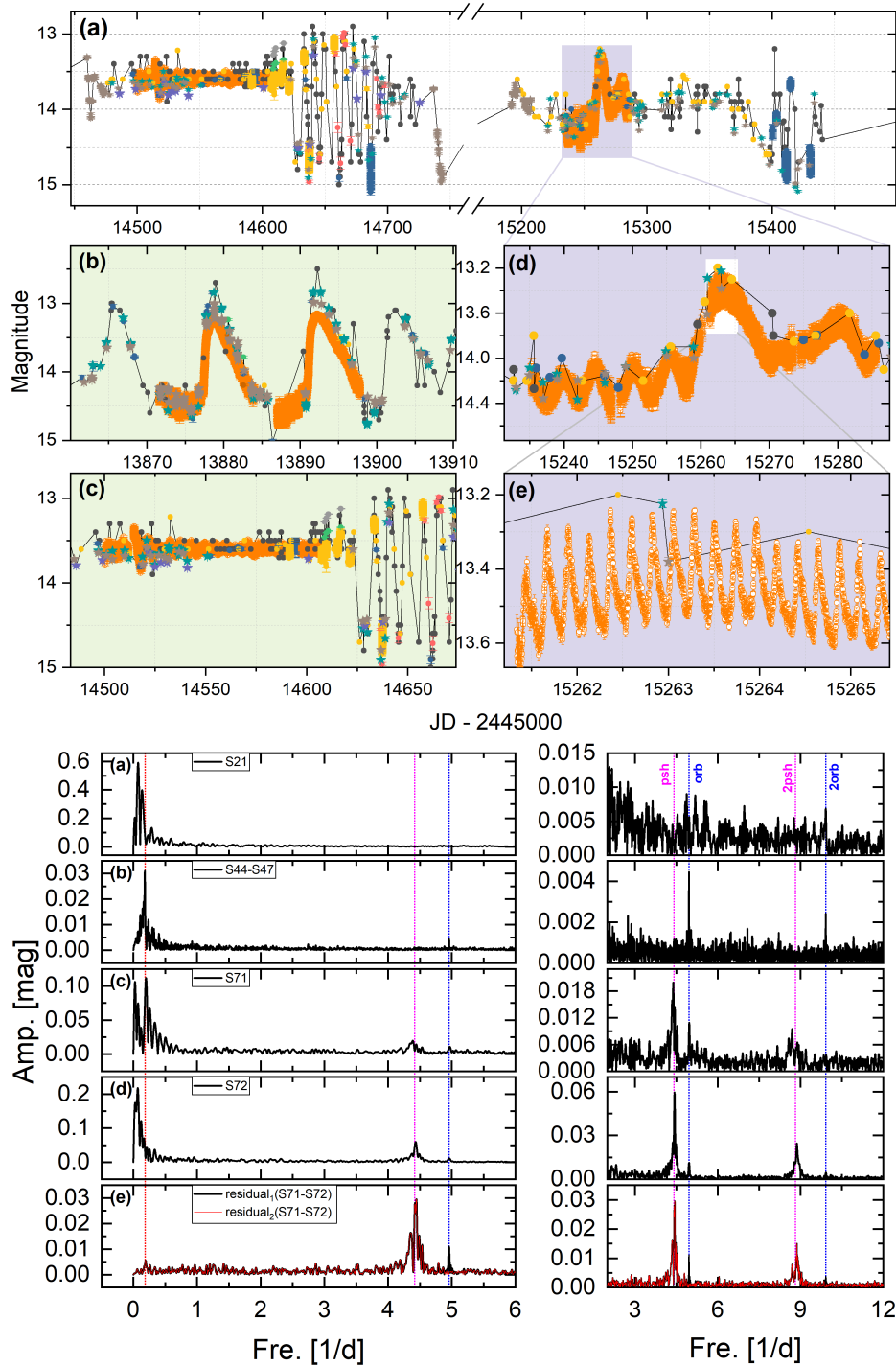
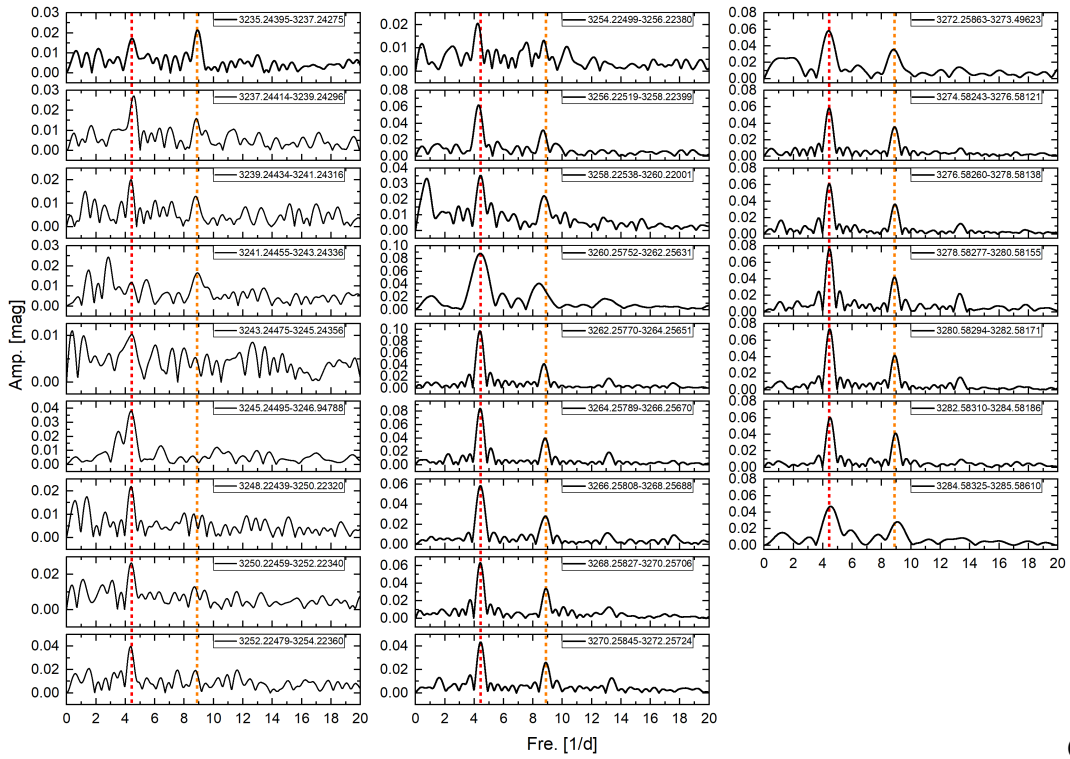
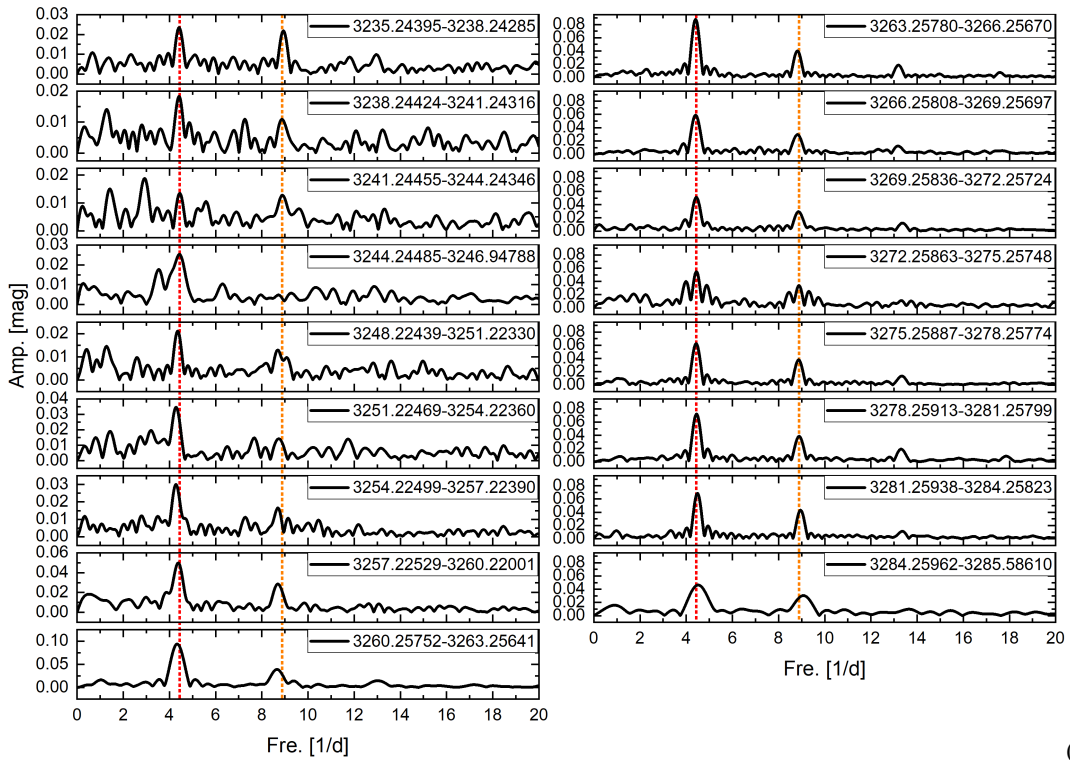


Figure A2. Top panels: (a) Part of the AT Cnc light curve from the localized magnification of Fig. A1; (b) Two short outbursts of AT Cnc were observed during S21; (c) Standstill during S44-S47; (d) Oscillations and superoutbursts during S71-S72; (e) Magnified image at the top of panel (d). Bottom panels: frequency spectra corresponding to S21, S44-S47, S71, S72, and S71-S72 in order of panels (a), (b), (c), (d), and (e). The black and red curves in panel (e) correspond to panels (b) and (c) in Fig. 1, and the right side is a partially enlarged view of the left side, where the vertical dashed lines correspond to the oscillatory frequency, PSH frequency, orbital frequency, twice the PSH harmonics, and twice the orbital harmonics.



(a)



(b)

Figure A4. Frequency spectra of segmented frequency analysis. (a) and (b) are the results of the segmented for 2 and 3 days analysis. The vertical dashed line in the figure corresponds to the PSH frequency and its second harmonic.

Table A6. Frequency analysis results for different sectors and segments.

Sectors/Spans -/TJD	Name	Fre. [1/d]	err [1/d]	Amp. [mag]	err [mag]	Phase [rad]	err [rad]
S21	2orb	9.9154	0.0014	0.0063	0.0004	0.41	0.07
S71	-	0.1978	0.0001	0.1119	0.0007	0.92	0.01
S71	psh	4.3872	0.0006	0.0177	0.0005	0.47	0.03
S71	orb	4.9589	0.0012	0.0093	0.0005	0.43	0.06
S71	2psh	8.6975	0.0011	0.0094	0.0005	0.48	0.05
S72	psh	4.4323	0.0002	0.0599	0.0005	0.79	0.01
S72	2psh	8.8673	0.0004	0.0239	0.0004	0.07	0.02
S72	orb	4.9545	0.0007	0.0111	0.0004	0.77	0.03
S72	2orb	9.9141	0.0017	0.0039	0.0003	0.38	0.08
S44-S47	-	0.1793	0.0001	0.0311	0.0002	0.77	0.01
S44-S47	orb	4.9562	0.0007	0.0046	0.0002	0.53	0.03
S44-S47	2orb	9.9133	0.0013	0.0025	0.0002	0.65	0.06
S71-S72	psh	4.4450	0.0003	0.0292	0.0004	0.19	0.01
S71-S72	2psh	8.8691	0.0005	0.0151	0.0004	0.18	0.02
S71-S72	orb	4.9566	0.0007	0.0102	0.0003	0.88	0.03
S71-S72	2orb	9.9136	0.0016	0.0039	0.0003	0.02	0.08
3235.24395-3237.24275	psh	4.464	0.027	0.0176	0.0017	0.70	0.10
3237.24414-3239.24296	psh	4.567	0.018	0.0271	0.0018	0.12	0.07
3239.24434-3241.24316	psh	4.382	0.022	0.0200	0.0016	0.33	0.08
3241.24455-3243.24336	psh	4.305	0.038	0.0115	0.0016	0.98	0.14
3243.24475-3245.24356	psh	4.428	0.040	0.0100	0.0015	0.17	0.15
3245.24495-3246.94788	psh	4.387	0.015	0.0380	0.0021	0.26	0.05
3248.22439-3250.22320	psh	4.388	0.021	0.0218	0.0016	0.14	0.08
3250.22459-3252.22340	psh	4.399	0.019	0.0265	0.0018	0.32	0.07
3252.22479-3254.22360	psh	4.357	0.017	0.0397	0.0024	0.72	0.06
3254.22499-3256.22380	psh	4.234	0.019	0.0205	0.0014	0.27	0.07
3256.22519-3258.22399	psh	4.295	0.009	0.0620	0.0021	0.71	0.03
3258.22538-3260.22001	psh	4.428	0.016	0.0353	0.0020	0.37	0.06
3260.25752-3262.25631	psh	4.408	0.008	0.0882	0.0027	0.21	0.03
3262.25770-3264.25651	psh	4.383	0.004	0.0976	0.0016	0.71	0.02
3264.25789-3266.25670	psh	4.403	0.005	0.0841	0.0015	0.45	0.02
3266.25808-3268.25688	psh	4.416	0.007	0.0584	0.0015	0.01	0.03
3268.25827-3270.25706	psh	4.409	0.007	0.0632	0.0017	0.88	0.03
3270.25845-3272.25724	psh	4.431	0.010	0.0435	0.0015	0.97	0.03
3272.25863-3273.49623	psh	4.394	0.014	0.0582	0.0029	0.06	0.05
3274.58243-3276.58121	psh	4.423	0.008	0.0582	0.0016	0.20	0.03
3276.58260-3278.58138	psh	4.434	0.007	0.0610	0.0015	0.17	0.03
3278.58277-3280.58155	psh	4.449	0.007	0.0763	0.0019	0.99	0.02
3280.58294-3282.58171	psh	4.464	0.006	0.0735	0.0015	0.76	0.02
3282.58310-3284.58186	psh	4.493	0.008	0.0601	0.0017	0.57	0.03
3284.58325-3285.58610	psh	4.532	0.013	0.0470	0.0023	0.48	0.05
3235.24395-3238.24285	psh	4.417	0.017	0.0235	0.0015	0.79	0.06
3238.24424-3241.24316	psh	4.417	0.020	0.0183	0.0014	0.92	0.07
3241.24455-3244.24346	psh	4.452	0.027	0.0138	0.0014	0.37	0.10
3244.24485-3246.94788	psh	4.434	0.017	0.0253	0.0015	0.68	0.06
3248.22439-3251.22330	psh	4.357	0.017	0.0211	0.0013	0.86	0.06
3251.22469-3254.22360	psh	4.288	0.014	0.0346	0.0018	0.21	0.05
3254.22499-3257.22390	psh	4.282	0.012	0.0300	0.0013	0.02	0.04
3257.22529-3260.22001	psh	4.380	0.010	0.0497	0.0018	0.80	0.04

Table A6 continued from previous page

Sectors/Spans -/TJD	Name	Fre. [1/d]	err [1/d]	Amp. [mag]	err [mag]	Phase [rad]	err [rad]
3260.25752-3263.25641	psh	4.336	0.005	0.0940	0.0017	0.06	0.02
3263.25780-3266.25670	psh	4.406	0.004	0.0877	0.0011	0.65	0.01
3266.25808-3269.25697	psh	4.408	0.006	0.0590	0.0012	0.15	0.02
3269.25836-3272.25724	psh	4.439	0.007	0.0510	0.0013	0.80	0.02
3272.25863-3275.25748	psh	4.443	0.011	0.0548	0.0021	0.69	0.04
3275.25887-3278.25774	psh	4.430	0.005	0.0626	0.0013	0.27	0.02
3278.25913-3281.25799	psh	4.448	0.005	0.0721	0.0013	0.27	0.02
3281.25938-3284.25823	psh	4.486	0.005	0.0686	0.0014	0.55	0.02
3284.25962-3285.58610	psh	4.519	0.012	0.0463	0.0021	0.19	0.04

Table A7. The outburst segments and the corresponding peak frequency parameters.

Start JD	End JD	Fre. [1/d]	err [1/d]	Period [d]	err [d]	Amp. [mag]	err [mag]	Phase [rad]	err [rad]
2449361.6940	2449517.6670	0.083	0.017	12.048	2.532	0.68	0.09	0.53	0.13
2450129.6510	2450244.6640	0.087	0.020	11.494	2.620	0.42	0.06	0.29	0.14
2450723.9750	2450967.8556	0.083	0.023	12.048	3.275	0.45	0.07	0.49	0.16
2451436.5800	2451699.7970	0.077	0.025	12.987	4.243	0.24	0.04	0.20	0.18
2452170.9830	2452427.8653	0.103	0.021	9.709	1.995	0.32	0.05	0.91	0.15
2453693.8468	2453860.7299	0.073	0.025	13.699	4.679	0.92	0.17	0.70	0.18
2454362.9830	2454599.6181	0.089	0.023	11.236	2.891	0.85	0.23	0.41	0.27
2454755.9314	2454980.4090	0.090	0.020	11.111	2.437	0.58	0.08	0.83	0.14
2455102.9650	2455264.4020	0.091	0.032	10.989	3.843	0.72	0.17	0.08	0.23
2455459.6563	2455716.5847	0.087	0.015	11.494	1.994	0.74	0.08	0.74	0.11
2455960.9193	2456084.6298	0.082	0.016	12.195	2.362	0.39	0.05	0.68	0.12
2456174.9238	2456452.6046	0.069	0.016	14.493	3.340	0.99	0.15	0.15	0.15
2456583.8564	2456818.6628	0.086	0.016	11.628	2.188	0.59	0.07	0.12	0.12
2456969.0636	2457172.6515	0.092	0.017	10.870	2.047	0.50	0.06	0.44	0.13
2457283.1386	2457430.8427	0.087	0.031	11.494	4.095	1.06	0.31	0.69	0.30
2457642.9225	2457737.9097	0.082	0.021	12.195	3.186	0.70	0.11	0.62	0.16
2457801.6109	2457901.5552	0.106	0.018	9.467	1.609	0.64	0.11	0.99	0.13
2458015.6361	2458146.7714	0.083	0.019	12.048	2.794	0.76	0.11	0.10	0.14
2458370.0221	2458522.3800	0.074	0.026	13.514	4.733	0.81	0.15	0.54	0.19
2458782.6111	2458995.3090	0.082	0.027	12.195	3.975	0.58	0.11	0.66	0.19
2459626.2632	2459725.6825	0.123	0.041	8.130	2.684	1.32	0.39	0.85	0.29

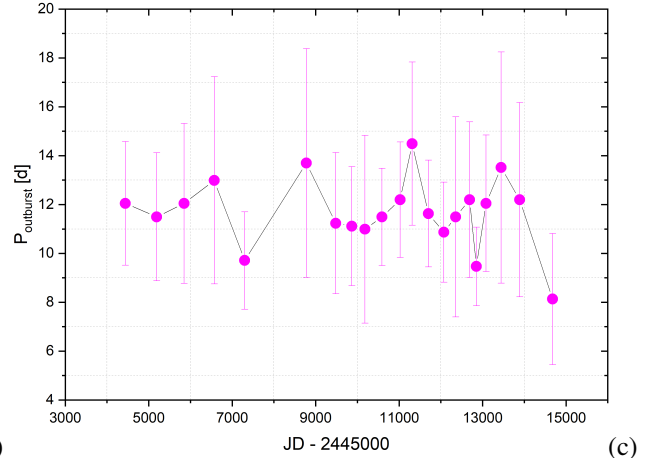
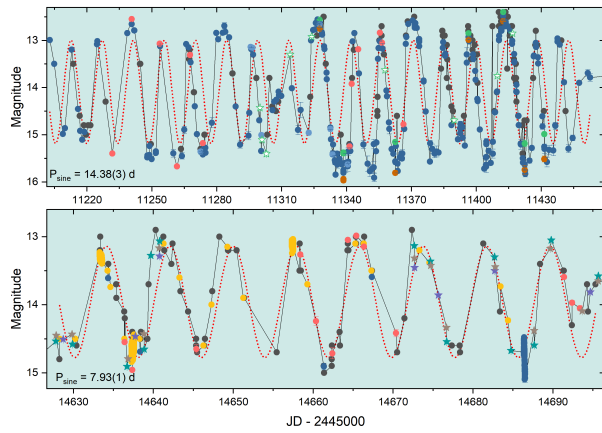
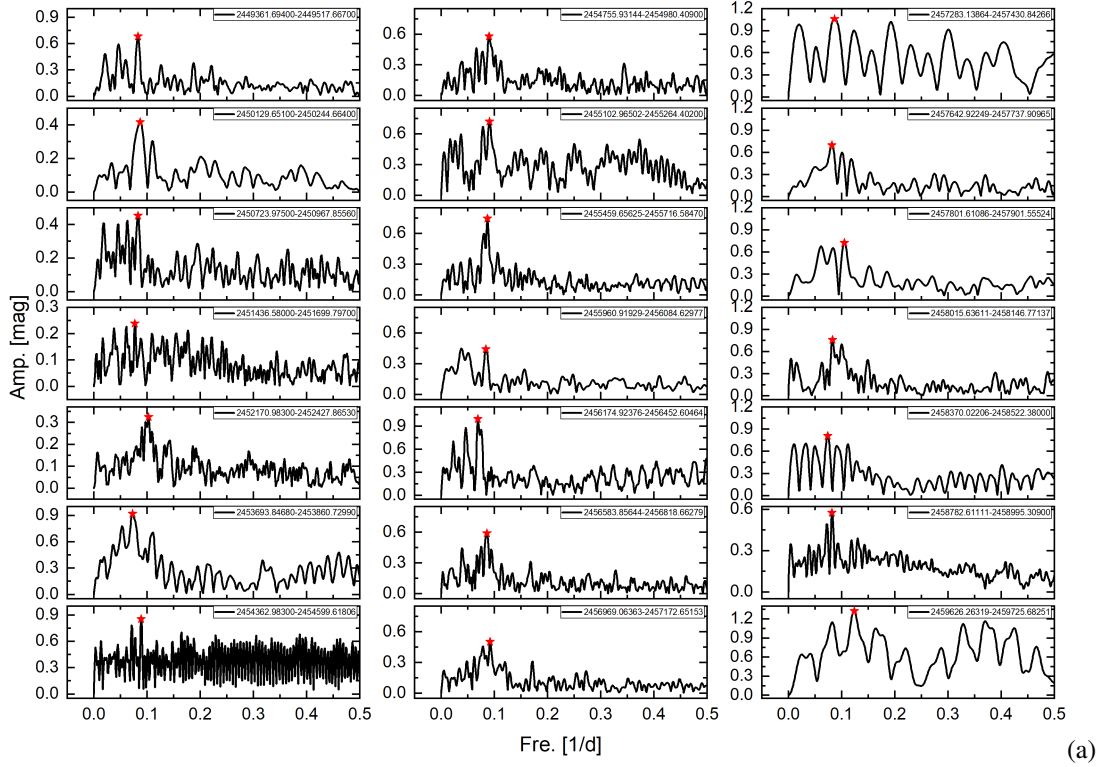


Figure A5. Analysis of the AT Cnc outburst periods. (a) Frequency spectra of the 21-segment outburst light curves, with the red pentagram corresponding to the peak frequency; (b) light curves corresponding to the longest and shortest outbursts and sine fits; (c) outburst period change curves.

References

- Balbus, S.A., Hawley, J.F., 1991. A Powerful Local Shear Instability in Weakly Magnetized Disks. I. Linear Analysis. *ApJ* 376, 214. doi:doi:[10.1086/170270](https://doi.org/10.1086/170270).
- Barrett, P., O'Donoghue, D., Warner, B., 1988. Photometry of the intermediate polar TV Columbae. *MNRAS* 233, 759–771. doi:doi:[10.1093/mnras/233.4.759](https://doi.org/10.1093/mnras/233.4.759).
- Bath, G.T., Evans, W.D., Papaloizou, J., Pringle, J.E., 1974. The accretion model of dwarf novae with application to Z Camelopardalis. *MNRAS* 169, 447–470. doi:doi:[10.1093/mnras/169.3.447](https://doi.org/10.1093/mnras/169.3.447).
- Bellm, E.C., Kulkarni, S.R., Graham, M.J., Dekany, R., Smith, R.M., Riddle, R., Masci, F.J., Helou, G., Prince, T.A., Adams, S.M., Barbarino, C., Barlow, T., Bauer, J., Beck, R., Belicki, J., Biswas, R., Blagorodnova, N., Bodewits, D., Bolin, B., Brinnel, V., Brooke, T., Bue, B., Bulla, M., Burruss, R., Cenko, S.B., Chang, C.K., Connolly, A., Coughlin, M., Cromer, J., Cunningham, V., De, K., Delacroix, A., Desai, V., Duev, D.A., Eadie, G., Farnham, T.L., Feeney, M., Feindt, U., Flynn, D., Franckowiak, A., Frederick, S., Fremling, C., Gal-Yam, A., Gezari, S., Giomi, M., Goldstein, D.A., Golkhou, V.Z., Goobar, A., Groom, S., Hacopians, E., Hale, D., Henning, J., Ho, A.Y.Q., Hover, D., Howell, J., Hung, T., Huppenkothen, D., Imel, D., Ip, W.H., Ivezić, Ž., Jackson, E., Jones, L., Juric, M., Kasliwal, M.M., Kaspi, S., Kaye, S., Kelley, M.S.P., Kowalski, M., Kramer, E., Kupfer, T., Landry, W., Laher, R.R., Lee, C.D., Lin, H.W., Lin, Z.Y., Lunnan, R., Giomi, M., Mahabal, A., Mao, P., Miller, A.A., Monkewitz, S., Murphy, P., Ngeow, C.C., Nordin, J., Nugent, P., Ofek, E., Patterson, M.T., Penprase, B., Porter, M., Rauch, L., Rebbapragada, U., Reiley, D., Rigault, M., Rodriguez, H., van Roestel, J., Rusholme, B., van Santen, J., Schulze, S., Shupe, D.L., Singer, L.P., Soumagnac, M.T., Stein, R., Surace, J., Sollerman, J., Szkody, P., Taddia, F., Terek, S., Van Sistine, A., van Velzen, S., Vestrand, W.T., Walters, R., Ward, C., Ye, Q.Z., Yu, P.C., Yan, L., Zolkower, J., 2019. The Zwicky Transient Facility: System Overview, Performance, and First Results. *PASP* 131, 018002. doi:doi:[10.1088/1538-3873/aaecbe](https://doi.org/10.1088/1538-3873/aaecbe), [arXiv:1902.01932](https://arxiv.org/abs/1902.01932).
- Bond, H.E., Tifft, W.G., 1974. A Spectroscopic Survey of Some High-Latitude Blue Variables. *PASP* 86, 981. doi:doi:[10.1086/129708](https://doi.org/10.1086/129708).
- Boneva, D., Yankova, K., Rusev, D., 2024. Periods of Outbursts and Standstills and Variations in Parameters of Two Z Cam Stars: Z Cam and AT Cnc. *Astronomy* 3, 208–219. doi:doi:[10.3390/astronomy3030013](https://doi.org/10.3390/astronomy3030013).
- Bruch, A., 2023. TESS light curves of cataclysmic variables - III - More superhump systems among old novae and nova-like variables. *MNRAS* 525, 1953–1975. doi:doi:[10.1093/mnras/stad2089](https://doi.org/10.1093/mnras/stad2089), [arXiv:2308.16106](https://arxiv.org/abs/2308.16106).
- Bruch, A., Boardman, J., Cook, L.M., Cook, M.J., Dvorak, S., Jones, J.L., Rock, J.W., Stone, G., Ulowetz, J.H., 2019. Coherent brightness modulations in the dwarf nova AT Cancri. *New A* 67, 22–28. doi:doi:[10.1016/j.newast.2018.09.001](https://doi.org/10.1016/j.newast.2018.09.001), [arXiv:1809.05640](https://arxiv.org/abs/1809.05640).
- Butters, O.W., West, R.G., Anderson, D.R., Collier Cameron, A., Clarkson, W.I., Enoch, B., Haswell, C.A., Hellier, C., Horne, K., Joshi, Y., Kane, S.R., Lister, T.A., Maxted, P.F.L., Parley, N., Pollacco, D., Smalley, B., Street, R.A., Todd, I., Wheatley, P.J., Wilson, D.M., 2010. The first WASP public data release. *A&A* 520, L10. doi:doi:[10.1051/0004-6361/201015655](https://doi.org/10.1051/0004-6361/201015655), [arXiv:1009.5306](https://arxiv.org/abs/1009.5306).
- Cleveland, W.S., 1979. Robust locally weighted regression and smoothing scatterplots. *Journal of the American statistical association* 74, 829–836.
- Court, J.M.C., Scaringi, S., Rappaport, S., Zhan, Z., Littlefield, C., Castro Segura, N., Knigge, C., Maccarone, T., Kennedy, M., Szkody, P., Garnavich, P., 2019. The eclipsing accreting white dwarf Z chameleontis as seen with TESS. *MNRAS* 488, 4149–4160. doi:doi:[10.1093/mnras/stz2015](https://doi.org/10.1093/mnras/stz2015), [arXiv:1907.08458](https://arxiv.org/abs/1907.08458).
- Dubus, G., Otulakowska-Hypka, M., Lasota, J.P., 2018. Testing the disk instability model of cataclysmic variables. *A&A* 617, A26. doi:doi:[10.1051/0004-6361/201833372](https://doi.org/10.1051/0004-6361/201833372).
- Gotz, W., 1983. Observations of AT Cnc in the Years 1982 and 1983. *Information Bulletin on Variable Stars* 2363, 1.
- Gotz, W., 1987. Optical Behaviour of AT Cancri in the Season 1986/87. *Information Bulletin on Variable Stars* 3066, 1.
- Götz, W., 1991. Optical behaviour of AT Cancri in the season 1990/91. *Zentralinstitut fuer Astrophysik Sternwarte Sonneberg Mitteilungen ueber Veraenderliche Sterne* 12, 111.

- Graham, M.J., Kulkarni, S.R., Bellm, E.C., Adams, S.M., Barbarino, C., Blagorodnova, N., Bodewits, D., Bolin, B., Brady, P.R., Cenko, S.B., Chang, C.K., Coughlin, M.W., De, K., Eadie, G., Farnham, T.L., Feindt, U., Franckowiak, A., Fremling, C., Gezari, S., Ghosh, S., Goldstein, D.A., Golkhou, V.Z., Goobar, A., Ho, A.Y.Q., Huppenkothen, D., Ivezić, Ž., Jones, R.L., Juric, M., Kaplan, D.L., Kasliwal, M.M., Kelley, M.S.P., Kupfer, T., Lee, C.D., Lin, H.W., Lunnan, R., Mahabal, A.A., Miller, A.A., Ngeow, C.C., Nugent, P., Ofek, E.O., Prince, T.A., Rauch, L., van Roestel, J., Schulze, S., Singer, L.P., Sollerman, J., Taddia, F., Yan, L., Ye, Q.Z., Yu, P.C., Barlow, T., Bauer, J., Beck, R., Belicki, J., Biswas, R., Brinnel, V., Brooke, T., Bue, B., Bulla, M., Burruss, R., Connolly, A., Cromer, J., Cunningham, V., Dekany, R., Delacroix, A., Desai, V., Duev, D.A., Feeney, M., Flynn, D., Frederick, S., Gal-Yam, A., Giomi, M., Groom, S., Hacopians, E., Hale, D., Helou, G., Henning, J., Hover, D., Hillenbrand, L.A., Howell, J., Hung, T., Imel, D., Ip, W.H., Jackson, E., Kaspi, S., Kaye, S., Kowalski, M., Kramer, E., Kuhn, M., Landry, W., Laher, R.R., Mao, P., Masci, F.J., Monkewitz, S., Murphy, P., Nordin, J., Patterson, M.T., Penprase, B., Porter, M., Rebbapragada, U., Reiley, D., Riddle, R., Rigault, M., Rodriguez, H., Rusholme, B., van Santen, J., Shupe, D.L., Smith, R.M., Soumagnac, M.T., Stein, R., Surace, J., Szkody, P., Terek, S., Van Sistine, A., van Velzen, S., Vestrand, W.T., Walters, R., Ward, C., Zhang, C., Zolkower, J., 2019. The Zwicky Transient Facility: Science Objectives. *PASP* 131, 078001. doi:doi:[10.1088/1538-3873/ab006c](https://doi.org/10.1088/1538-3873/ab006c), [arXiv:1902.01945](https://arxiv.org/abs/1902.01945).
- Hameury, J.M., 2020. A review of the disc instability model for dwarf novae, soft X-ray transients and related objects. *Advances in Space Research* 66, 1004–1024. doi:doi:[10.1016/j.asr.2019.10.022](https://doi.org/10.1016/j.asr.2019.10.022), [arXiv:1910.01852](https://arxiv.org/abs/1910.01852).
- Hameury, J.M., Lasota, J.P., 2014. Anomalous Z Cam stars: a response to mass-transfer outbursts. *A&A* 569, A48. doi:doi:[10.1051/0004-6361/201424535](https://doi.org/10.1051/0004-6361/201424535), [arXiv:1407.3156](https://arxiv.org/abs/1407.3156).
- Harvey, D., Skillman, D.R., Patterson, J., Ringwald, F., 1995. Superhumps in cataclysmic binaries. v. v503 cygni. *PASP* 107, 551. doi:doi:[10.1086/133591](https://doi.org/10.1086/133591).
- Hellier, C., 2001. On Echo Outbursts and ER UMa Supercycles in SU UMa-Type Cataclysmic Variables. *PASP* 113, 469–472. doi:doi:[10.1086/319540](https://doi.org/10.1086/319540), [arXiv:astro-ph/0101102](https://arxiv.org/abs/astro-ph/0101102).
- Honeycutt, R.K., Robertson, J.W., Turner, G.W., Mattei, J.A., 1998. Are Z Camelopardalis-Type Dwarf Novae Brighter at Standstill? *PASP* 110, 676–688. doi:doi:[10.1086/316180](https://doi.org/10.1086/316180).
- Howell, S.B., Szkody, P., Cannizzo, J.K., 1995. Tremendous Outburst Amplitude Dwarf Novae. *Astrophysical Journal* 439, 337. doi:doi:[10.1086/175177](https://doi.org/10.1086/175177).
- Jayasinghe, T., Stanek, K.Z., Kochanek, C.S., Shappee, B.J., Holoien, T.W.S., Thompson, T.A., Prieto, J.L., Dong, S., Pawlak, M., Pejcha, O., Shields, J.V., Pojmanski, G., Otero, S., Britt, C.A., Will, D., 2019. The ASAS-SN catalogue of variable stars - II. Uniform classification of 412 000 known variables. *MNRAS* 486, 1907–1943. doi:doi:[10.1093/mnras/stz844](https://doi.org/10.1093/mnras/stz844), [arXiv:1809.07329](https://arxiv.org/abs/1809.07329).
- Jenkins, J.M., Twicken, J.D., McCauliff, S., Campbell, J., Sanderfer, D., Lung, D., Mansouri-Samani, M., Girouard, F., Tenenbaum, P., Klaus, T., Smith, J.C., Caldwell, D.A., Chacon, A.D., Henze, C., Heiges, C., Latham, D.W., Morgan, E., Swade, D., Rinehart, S., Vanderspek, R., 2016. The TESS science processing operations center, in: Chiozzi, G., Guzman, J.C. (Eds.), *Software and Cyberinfrastructure for Astronomy IV*, p. 99133E. doi:doi:[10.1117/12.2233418](https://doi.org/10.1117/12.2233418).
- Kato, T., 2019. Three Z Camelopardalis-type dwarf novae exhibiting IW Andromedae-type phenomenon. *PASJ* 71, 20. doi:doi:[10.1093/pasj/psy138](https://doi.org/10.1093/pasj/psy138), [arXiv:1811.05038](https://arxiv.org/abs/1811.05038).
- Kato, T., 2022. Analysis of TESS observations of V844 Her during the 2020 superoutburst. *arXiv e-prints*, [arXiv:2205.05284](https://arxiv.org/abs/2205.05284)doi:doi:[10.48550/arXiv.2205.05284](https://doi.org/10.48550/arXiv.2205.05284), [arXiv:2205.05284](https://arxiv.org/abs/2205.05284).
- Kato, T., Hamsch, F.J., Dubovsky, P.A., Kudzej, I., Monard, B., Miller, I., Itoh, H., Kiyota, S., Masumoto, K., Fukushima, D., et al., 2015. Survey of period variations of superhumps in su uma-type dwarf novae. vii. the seventh year (2014–2015). *PASJ* 67, 105.
- Kato, T., Imada, A., Uemura, M., Nogami, D., Maehara, H., Ishioka, R., Baba, H., Matsumoto, K., Iwamatsu, H., Kubota, K., Sugiyasu, K., Soejima, Y., Moritani, Y., Ohshima, T., Ohashi, H., Tanaka, J., Sasada, M., Arai, A., Nakajima, K., Kiyota, S., Tanabe, K., Imamura, K., Kunitomi, N., Kunihiro, K., Taguchi, H., Koizumi, M., Yamada, N., Nishi, Y., Kida, M., Tanaka, S., Ueoka, R., Yasui, H., Maruoka, K., Henden, A., Oksanen, A., Moilanen, M., Tikkanen, P., Aho, M., Monard, B., Itoh, H., Dubovsky, P.A., Kudzej, I., Dancikova, R., Vanmunster, T., Pietz, J., Bolt, G., Boyd, D., Nelson, P., Krajci, T., Cook, L.M., Torii, K., Starkey, D.R., Shears, J., Jensen, L.T., Masi, G., Hrynek, T., Novák, R., Kocián, R., Král, L., Kučáková, H., Kolasa, M., Štastný, P., Staels, B., Miller, I., Sano, Y., Ponthière, P.d., Miyashita, A., Crawford, T., Brady, S., Santallo, R., Richards,

- T., Martin, B., Buczynski, D., Richmond, M., Kern, J., Davis, S., Crabtree, D., Beaulieu, K., Davis, T., Aggleton, M., Morelle, E., Pavlenko, E.P., Andreev, M., Baklanov, A., Koppelman, M.D., Billings, G., Urbančok, L., Ögmen, Y., Heathcote, B., Gomez, T.L., Voloshina, I., Retter, A., Mularczyk, K., Złoczewski, K., Olech, A., Kedzierski, P., Pickard, R.D., Stockdale, C., Virtanen, J., Morikawa, K., Hamsch, F.J., Garradd, G., Gualdoni, C., Geary, K., Omodaka, T., Sakai, N., Michel, R., Cárdenas, A.A., Gazeas, K.D., Niarchos, P.G., Yushchenko, A.V., Mallia, F., Fiaschi, M., Good, G.A., Walker, S., James, N., Douzu, K.i., Julian, W.M., Butterworth, N.D., Shugarov, S.Y., Volkov, I., Chochol, D., Katysheva, N., Rosenbush, A.E., Khramtsova, M., Kehusmaa, P., Reszelski, M., Bedient, J., Liller, W., Pojmański, G., Simonsen, M., Stubbings, R., Schmeer, P., Muylaert, E., Kinnunen, T., Poyner, G., Ripero, J., Kriebel, W., 2009. Survey of Period Variations of Superhumps in SU UMa-Type Dwarf Novae. *PASJ* 61, S395–S616. doi:doi:[10.1093/pasj/61.sp2.S395](https://doi.org/10.1093/pasj/61.sp2.S395), [arXiv:0905.1757](https://arxiv.org/abs/0905.1757).
- Kato, T., Kojiguchi, N., 2021. Orbital period of the IW And-type star ST Cha. arXiv e-prints , arXiv:2112.08552doi:doi:[10.48550/arXiv.2112.08552](https://doi.org/10.48550/arXiv.2112.08552), [arXiv:2112.08552](https://arxiv.org/abs/2112.08552).
- Kato, T., Maehara, H., Miller, I., Ohshima, T., de Miguel, E., Tanabe, K., Imamura, K., Akazawa, H., Kunitomi, N., Takagi, R., Nose, M., Hamsch, F.J., Kiyota, S., Pavlenko, E.P., Baklanov, A.V., Antonyuk, O.I., Samsonov, D., Sosnovskij, A., Antonyuk, K., Andreev, M.V., Morelle, E., Dubovsky, P.A., Kudzej, I., Oksanen, A., Masi, G., Krajci, T., Pickard, R.D., Sabo, R., Itoh, H., Stein, W., Dvorak, S., Henden, A., Nakagawa, S., Noguchi, R., Iino, E., Matsumoto, K., Nishitani, H., Aoki, T., Kobayashi, H., Akasaka, C., Bolt, G., Shears, J., Ruiz, J., Shugarov, S.Y., Chochol, D., Parakhin, N.A., Monard, B., Shiokawa, K., Kasai, K., Staels, B., Miyashita, A., Starkey, D.R., Ögmen, Y., Littlefield, C., Katysheva, N., Sergey, I.M., Denisenko, D., Tordai, T., Fidrich, R., Goranskij, V.P., Virtanen, J., Crawford, T., Pietz, J., Koff, R.A., Boyd, D., Brady, S., James, N., Goff, W.N., Itagaki, K.I., Nishimura, H., Nakashima, Y., Yoshida, S., Stubbings, R., Poyner, G., Maeda, Y., Korotkiy, S.A., Sokolovsky, K.V., Ueda, S., 2012. Survey of Period Variations of Superhumps in SU UMa-Type Dwarf Novae. III. The Third Year (2010-2011). *PASJ* 64, 21. doi:doi:[10.1093/pasj/64.1.21](https://doi.org/10.1093/pasj/64.1.21), [arXiv:1108.5252](https://arxiv.org/abs/1108.5252).
- Kato, T., Maehara, H., Monard, B., 2008. Late Superhumps in WZ Sge-Type Dwarf Novae. *PASJ* 60, L23. doi:doi:[10.1093/pasj/60.4.L23](https://doi.org/10.1093/pasj/60.4.L23), [arXiv:0806.4248](https://arxiv.org/abs/0806.4248).
- Kato, T., Pavlenko, E.P., Pit, N.V., Antonyuk, K.A., Antonyuk, O.I., Babina, J.V., Baklanov, A.V., Sosnovskij, A.A., Belan, S.P., Maeda, Y., Sugiura, Y., Sumiya, S., Matsumoto, H., Ito, D., Nikai, K., Kojiguchi, N., Matsumoto, K., Dubovsky, P.A., Kudzej, I., Medulka, T., Wakamatsu, Y., Ohnishi, R., Seki, T., Isogai, K., Simon, A.O., Romanjuk, Y.O., Baransky, A.R., Sergeev, A.V., Godunova, V.G., Izviakova, I.O., Kozlov, V.A., Sklyanov, A.S., Zhuchkov, R.Y., Gutaev, A.G., Ponomarenko, V.O., Vasylenko, V.V., Miller, I., Kasai, K., Dvorak, S., Menzies, K., de Miguel, E., Brincat, S.M., Pickard, R.D., 2019. Discovery of standstills in the SU UMa-type dwarf nova NY Serpentis. *PASJ* 71, L1. doi:doi:[10.1093/pasj/psz007](https://doi.org/10.1093/pasj/psz007), [arXiv:1901.05100](https://arxiv.org/abs/1901.05100).
- Kato, T., Stubbings, R., Reszelski, M., Muylaert, E., Simonsen, M., Poyner, G., Dubovsky, P.A., Pearce, A., Kinnunen, T., Maehara, H., 2001. Unusual Slow Fading of Standstill in AT Cnc. *Information Bulletin on Variable Stars* 5099, 1.
- Kato, T., Tampo, Y., Kojiguchi, N., Shibata, M., Ito, J., Isogai, K., Itoh, H., Hamsch, F.J., Monard, B., Kiyota, S., Vanmunster, T., Sosnovskij, A.A., Pavlenko, E.P., Dubovsky, P.A., Kudzej, I., Medulka, T., 2021. BO Ceti: Dwarf nova showing both IW And-type and SU UMa-Type features. *PASJ* 73, 1280–1288. doi:doi:[10.1093/pasj/psab074](https://doi.org/10.1093/pasj/psab074), [arXiv:2106.15028](https://arxiv.org/abs/2106.15028).
- Kato, T., Wakamatsu, Y., Kojiguchi, N., Kimura, M., Ohnishi, R., Isogai, K., Nijjima, K., Yoshitake, T., Sugiura, Y., Sumiya, S., Ito, D., Nikai, K., Matsumoto, H., Matsumoto, K., Vanmunster, T., Hamsch, F.J., Itoh, H., Babina, J.V., Antonyuk, O.I., Baklanov, A.V., Pavlenko, E.P., Monard, B., Dvorak, S., 2020. IW And-type state in IM Eridani. *PASJ* 72, 11. doi:doi:[10.1093/pasj/psz130](https://doi.org/10.1093/pasj/psz130), [arXiv:1911.01587](https://arxiv.org/abs/1911.01587).
- Katz, J.I., 1973. Thirty-five-day Periodicity in Her X-1. *Nature Physical Science* 246, 87–89. doi:doi:[10.1038/physci246087a0](https://doi.org/10.1038/physci246087a0).
- Kimura, M., Osaki, Y., Kato, T., 2020a. KIC 9406652: A laboratory for tilted disks in cataclysmic variable stars. *PASJ* 72, 94. doi:doi:[10.1093/pasj/psaa088](https://doi.org/10.1093/pasj/psaa088), [arXiv:2008.11328](https://arxiv.org/abs/2008.11328).
- Kimura, M., Osaki, Y., Kato, T., Mineshige, S., 2020b. Thermal-viscous instability in tilted accretion disks: A possible application to iw andromeda-type dwarf novae. *PASJ* 72, 22. doi:doi:[10.1093/pasj/psj144](https://doi.org/10.1093/pasj/psj144).
- Kinemuchi, K., Barclay, T., Fanelli, M., Pepper, J., Still, M., Howell, S.B., 2012. Demystifying Kepler Data: A Primer for Systematic Artifact Mitigation. *PASP* 124, 963. doi:doi:[10.1086/667603](https://doi.org/10.1086/667603), [arXiv:1207.3093](https://arxiv.org/abs/1207.3093).
- Knigge, C., King, A.R., Patterson, J., 2000. Assisted stellar suicide: the wind-driven evolution of the recurrent nova T Pyxidis. *A&A* 364, L75–L79. doi:doi:[10.48550/arXiv.astro-ph/0011304](https://doi.org/10.48550/arXiv.astro-ph/0011304), [arXiv:astro-ph/0011304](https://arxiv.org/abs/astro-ph/0011304).

- Kochanek, C.S., Shappee, B.J., Stanek, K.Z., Holoiien, T.W.S., Thompson, T.A., Prieto, J.L., Dong, S., Shields, J.V., Will, D., Britt, C., Perzanowski, D., Pojmański, G., 2017. The All-Sky Automated Survey for Supernovae (ASAS-SN) Light Curve Server v1.0. *PASP* 129, 104502. doi:doi:[10.1088/1538-3873/aa80d9](https://doi.org/10.1088/1538-3873/aa80d9), [arXiv:1706.07060](https://arxiv.org/abs/1706.07060).
- Kozhevnikov, V.P., 2004. Detection of superhumps in the Z Camelopardalis-type dwarf nova <ASTROBJ>AT Cnc</ASTROBJ> at standstill. *A&A* 419, 1035–1044. doi:doi:[10.1051/0004-6361:20035600](https://doi.org/10.1051/0004-6361:20035600).
- Lasota, J.P., 2001. The disc instability model of dwarf novae and low-mass x-ray binary transients. *New Astronomy Reviews* 45, 449–508. doi:doi:[10.1016/S1387-6473\(01\)00112-9](https://doi.org/10.1016/S1387-6473(01)00112-9).
- Lenz, P., Breger, M., 2005. Period04 User Guide. *Communications in Asteroseismology* 146, 53–136. doi:doi:[10.1553/cia146s53](https://doi.org/10.1553/cia146s53).
- Lin, D.N.C., Papaloizou, J., Faulkner, J., 1985. On the evolution of accretion disc flow in cataclysmic variables - III. Outburst properties of constant and uniform -alpha model discs. *MNRAS* 212, 105–149. doi:doi:[10.1093/mnras/212.1.105](https://doi.org/10.1093/mnras/212.1.105).
- Lubow, S.H., 1991. A Model for Tidally Driven Eccentric Instabilities in Fluid Disks. *ApJ* 381, 259. doi:doi:[10.1086/170647](https://doi.org/10.1086/170647).
- Marino, B.F., Walker, W.S.G., 1974. An Orbital Period for VW Hydri. *Information Bulletin on Variable Stars* 864, 1.
- Masci, F.J., Laher, R.R., Rusholme, B., Shupe, D.L., Groom, S., Surace, J., Jackson, E., Monkewitz, S., Beck, R., Flynn, D., Terek, S., Landry, W., Hacopians, E., Desai, V., Howell, J., Brooke, T., Imel, D., Wachter, S., Ye, Q.Z., Lin, H.W., Cenko, S.B., Cunningham, V., Rebbapragada, U., Bue, B., Miller, A.A., Mahabal, A., Bellm, E.C., Patterson, M.T., Jurić, M., Golkhou, V.Z., Ofek, E.O., Walters, R., Graham, M., Kasliwal, M.M., Dekany, R.G., Kupfer, T., Burdge, K., Cannella, C.B., Barlow, T., Van Sistine, A., Giomi, M., Fremling, C., Blagorodnova, N., Levitan, D., Riddle, R., Smith, R.M., Helou, G., Prince, T.A., Kulkarni, S.R., 2019. The Zwicky Transient Facility: Data Processing, Products, and Archive. *PASP* 131, 018003. doi:doi:[10.1088/1538-3873/aae8ac](https://doi.org/10.1088/1538-3873/aae8ac), [arXiv:1902.01872](https://arxiv.org/abs/1902.01872).
- Meyer, F., Meyer-Hofmeister, E., 1983. A model for the standstill of the Z Camelopardalis variables. *A&A* 121, 29–34.
- Mineshige, S., Osaki, Y., 1983. Disk-instability model for outbursts of dwarf novae Time-dependent formulation and one-zone model. *PASJ* 35, 377–396.
- Murray, J., Warner, B., Wickramasinghe, D., 2000. Superhumps in systems with intermediate mass ratios. *New A Rev.* 44, 51–56. doi:doi:[10.1016/S1387-6473\(00\)00013-0](https://doi.org/10.1016/S1387-6473(00)00013-0).
- Murray, J.R., 2000. The precession of eccentric discs in close binaries. *MNRAS* 314, L1–L5. doi:doi:[10.1046/j.1365-8711.2000.03424.x](https://doi.org/10.1046/j.1365-8711.2000.03424.x), [arXiv:astro-ph/9911466](https://arxiv.org/abs/astro-ph/9911466).
- Nogami, D., Masuda, S., Kato, T., Hirata, R., 1999. Spectroscopic and Photometric Observations of a Z Cam-Type Dwarf Nova, AT Cancri, in Standstill. *PASJ* 51, 115–125. doi:doi:[10.1093/pasj/51.1.115](https://doi.org/10.1093/pasj/51.1.115).
- Osaki, Y., 1974. An Accretion Model for the Outbursts of U Geminorum Stars. *PASJ* 26, 429.
- Osaki, Y., 1985. Irradiation-induced mass-overflow instability as a possible cause of superoutbursts in su uma stars. *A&A* 144, 369–380.
- Osaki, Y., 1989. A model for the superoutburst phenomenon of SU Ursae MAjoris stars. *Publications of the Astronomical Society of Japan* 41, 1005–1033.
- Osaki, Y., 2005. The disk instability model for dwarf nova outbursts. *Proceedings of the Japan Academy, Series B* 81, 291–305. doi:doi:[10.2183/pjab.81.291](https://doi.org/10.2183/pjab.81.291).
- Osaki, Y., Meyer, F., 2003. Is evidence for enhanced mass transfer during dwarf-nova outbursts well substantiated? *A&A* 401, 325–337. doi:doi:[10.1051/0004-6361:20030115](https://doi.org/10.1051/0004-6361:20030115), [arXiv:astro-ph/0302140](https://arxiv.org/abs/astro-ph/0302140).
- Paczynski, B., 1977. A model of accretion disks in close binaries. *Astrophysical Journal* 216, 822–826. doi:doi:[10.1086/155526](https://doi.org/10.1086/155526).
- Papaloizou, J., Pringle, J.E., 1979. A model for the superhumps in cataclysmic variables. *MNRAS* 189, 293–297. doi:doi:[10.1093/mnras/189.2.293](https://doi.org/10.1093/mnras/189.2.293).

- Patterson, J., Kemp, J., Harvey, D.A., Fried, R.E., Rea, R., Monard, B., Cook, L.M., Skillman, D.R., Vanmunster, T., Bolt, G., Armstrong, E., McCormick, J., Krajci, T., Jensen, L., Gunn, J., Butterworth, N., Foote, J., Bos, M., Masi, G., Warhurst, P., 2005. Superhumps in Cataclysmic Binaries. XXV. q_{crit} , $\epsilon(q)$, and Mass-Radius. *PASP* 117, 1204–1222. doi:doi:[10.1086/447771](https://doi.org/10.1086/447771), [arXiv:astro-ph/0507371](https://arxiv.org/abs/astro-ph/0507371).
- Polikar, R., et al., 1996. The wavelet tutorial.
- Pollacco, D.L., Skillen, I., Collier Cameron, A., Christian, D.J., Hellier, C., Irwin, J., Lister, T.A., Street, R.A., West, R.G., Anderson, D.R., Clarkson, W.I., Deeg, H., Enoch, B., Evans, A., Fitzsimmons, A., Haswell, C.A., Hodgkin, S., Horne, K., Kane, S.R., Keenan, F.P., Maxted, P.F.L., Norton, A.J., Osborne, J., Parley, N.R., Ryans, R.S.I., Smalley, B., Wheatley, P.J., Wilson, D.M., 2006. The WASP Project and the SuperWASP Cameras. *PASP* 118, 1407–1418. doi:doi:[10.1086/508556](https://doi.org/10.1086/508556), [arXiv:astro-ph/0608454](https://arxiv.org/abs/astro-ph/0608454).
- Ricker, G., Winn, J., Vanderspek, R., 2015. Journal of astronomical telescopes, instruments, and systems. *JATIS* 1, 014003. doi:doi:[10.1117/1.JATIS.1.1.014003](https://doi.org/10.1117/1.JATIS.1.1.014003).
- Romano, G., Perssinotto, M., 1968. *Publ. Astr. Obs. Padova* 151, 9.
- Shappee, B.J., Prieto, J.L., Grupe, D., Kochanek, C.S., Stanek, K.Z., De Rosa, G., Mathur, S., Zu, Y., Peterson, B.M., Pogge, R.W., Komossa, S., Im, M., Jencson, J., Holoiien, T.W.S., Basu, U., Beacom, J.F., Szczygieł, D.M., Brimacombe, J., Adams, S., Campillay, A., Choi, C., Contreras, C., Dietrich, M., Dubberley, M., Elphick, M., Foale, S., Giustini, M., Gonzalez, C., Hawkins, E., Howell, D.A., Hsiao, E.Y., Koss, M., Leighly, K.M., Morrell, N., Mudd, D., Mullins, D., Nugent, J.M., Parrent, J., Phillips, M.M., Pojmanski, G., Rosing, W., Ross, R., Sand, D., Terndrup, D.M., Valenti, S., Walker, Z., Yoon, Y., 2014. The Man behind the Curtain: X-Rays Drive the UV through NIR Variability in the 2013 Active Galactic Nucleus Outburst in NGC 2617. *ApJ* 788, 48. doi:doi:[10.1088/0004-637X/788/1/48](https://doi.org/10.1088/0004-637X/788/1/48), [arXiv:1310.2241](https://arxiv.org/abs/1310.2241).
- Shara, M.M., Drissen, L., Martin, T., Alarie, A., Stephenson, F.R., 2017. When does an old nova become a dwarf nova? Kinematics and age of the nova shell of the dwarf nova AT Cancri. *MNRAS* 465, 739–745. doi:doi:[10.1093/mnras/stw2753](https://doi.org/10.1093/mnras/stw2753), [arXiv:1609.06695](https://arxiv.org/abs/1609.06695).
- Shara, M.M., Mizusawa, T., Wehinger, P., Zurek, D., Martin, C.D., Neill, J.D., Forster, K., Seibert, M., 2012. AT Cnc: A Second Dwarf Nova with a Classical Nova Shell. *ApJ* 758, 121. doi:doi:[10.1088/0004-637X/758/2/121](https://doi.org/10.1088/0004-637X/758/2/121), [arXiv:1208.1280](https://arxiv.org/abs/1208.1280).
- Simonsen, M., 2011. The Z CamPaign Early Results, in: American Astronomical Society Meeting Abstracts #218, p. 103.02.
- Smak, J., 1983. On the nature of dwarf novae. *ApJ* 272, 234–237. doi:doi:[10.1086/161284](https://doi.org/10.1086/161284).
- Smak, J., 1995. Observational Evidence for the Enhancement of the Mass Transfer Rate during Dwarf Nova Outbursts. *Acta Astron.* 45, 355–360.
- Sun, Q.B., Qian, S.B., Li, M.Y., 2023c. Evolution of Negative Superhumps, Quasiperiodic Oscillations, and Outbursts in the Z Cam-type Dwarf Nova AH Her. *ApJ* 955, 135. doi:doi:[10.3847/1538-4357/ace183](https://doi.org/10.3847/1538-4357/ace183), [arXiv:2309.05891](https://arxiv.org/abs/2309.05891).
- Sun, Q.B., Qian, S.B., Zhu, L.Y., Dong, A.J., Zhi, Q.J., Liao, W.P., Zhao, E.G., Han, Z.T., Liu, W., Zang, L., Li, F.X., Shi, X.D., 2023a. First discovery of quasi-periodic oscillations in the dwarf nova HS 2325+8205 based on TESS photometry. *MNRAS* 518, 3901–3907. doi:doi:[10.1093/mnras/stac3272](https://doi.org/10.1093/mnras/stac3272), [arXiv:2302.05887](https://arxiv.org/abs/2302.05887).
- Sun, Q.B., Qian, S.B., Zhu, L.Y., Li, Q.M., Li, F.X., Li, M.Y., Li, P., 2024d. A new iw and-type star: Karachurin 12 with tilted disks and diverse cycles. *ApJ* 976, 107. URL: <https://dx.doi.org/10.3847/1538-4357/ad8446>, doi:doi:[10.3847/1538-4357/ad8446](https://doi.org/10.3847/1538-4357/ad8446).
- Sun, Q.B., Qian, S.B., Zhu, L.Y., Li, Q.M., Li, M.Y., Li, P., 2024c. Tilted Disk Precession and Negative Superhumps in HS 2325+8205: A Multiwindow Analysis. *ApJ* 974, 132. doi:doi:[10.3847/1538-4357/ad6f05](https://doi.org/10.3847/1538-4357/ad6f05), [arXiv:2407.04913](https://arxiv.org/abs/2407.04913).
- Sun, Q.B., Qian, S.B., Zhu, L.Y., Liao, W.P., Zhao, E.G., Li, F.X., Shi, X.D., Li, M.Y., 2023b. New evidence for the precession of tilted disk in SDSS J081256.85+191157.8. *MNRAS* 526, 3730–3743. doi:doi:[10.1093/mnras/stad1880](https://doi.org/10.1093/mnras/stad1880), [arXiv:2303.11847](https://arxiv.org/abs/2303.11847).
- Sun, Q.B., Qian, S.B., Zhu, L.Y., Liao, W.P., Zhao, E.G., Li, F.X., Shi, X.D., Li, M.Y., 2024a. Nine New Cataclysmic Variable Stars with Negative Superhumps. *ApJ* 962, 123. doi:doi:[10.3847/1538-4357/ad0f1c](https://doi.org/10.3847/1538-4357/ad0f1c), [arXiv:2309.11033](https://arxiv.org/abs/2309.11033).

- Sun, Q.B., Qian, S.B., Zhu, L.Y., Liao, W.P., Zhao, E.G., Li, F.X., Shi, X.D., Li, M.Y., 2024b. A New Window for Studying Intermediate Polars and Tilted Accretion Disk Precession. *ApJ* 966, 83. doi:doi:[10.3847/1538-4357/ad2fc2](https://doi.org/10.3847/1538-4357/ad2fc2), [arXiv:2401.08162](https://arxiv.org/abs/2401.08162).
- Twicken, J.D., Chandrasekaran, H., Jenkins, J.M., Gunter, J.P., Girouard, F., Klaus, T.C., 2010. Presearch data conditioning in the Kepler Science Operations Center pipeline, in: Radziwill, N.M., Bridger, A. (Eds.), *Software and Cyberinfrastructure for Astronomy*, p. 77401U. doi:doi:[10.1117/12.856798](https://doi.org/10.1117/12.856798).
- Vogt, N., 1974. Photometric study of the dwarf nova VW Hydri. *A&A* 36, 369–378.
- Vogt, N., 1982. Z chamaeleontis-evidence for an eccentric disk during supermaximum. *ApJ* 252, 653–667. doi:doi:[10.1086/159592](https://doi.org/10.1086/159592).
- Wakamatsu, Y., Thorstensen, J.R., Kojiguchi, N., Isogai, K., Kimura, M., Ohnishi, R., Kato, T., Itoh, H., Sugiura, Y., Sumiya, S., Matsumoto, H., Ito, D., Nikai, K., Akitaya, H., Ishioka, C., Oide, K., Kanai, T., Uzawa, Y., Oasa, Y., Tordai, T., Vanmunster, T., Shugarov, S.Y., Yamanaka, M., Sasada, M., Takagi, K., Nishinaka, Y., Yamazaki, Y., Otsubo, I., Nakaoka, T., Murata, K.L., Ohsawa, R., Morita, M., Ichiki, M., Dufoer, S., Mizutani, M., Horiuchi, T., Tozuka, M., Takayama, M., Ohshima, T., Saito, T., Dubovsky, P.A., Stone, G., Miller, I., Nogami, D., 2021. ASASSN-18aan: An eclipsing SU UMa-type cataclysmic variable with a 3.6-hr orbital period and a late G-type secondary star. *PASJ* 73, 1209–1224. doi:doi:[10.1093/pasj/psab003](https://doi.org/10.1093/pasj/psab003), [arXiv:2102.04104](https://arxiv.org/abs/2102.04104).
- Warner, B., 1985. Stars That Go Hump in the Night: The SU UMa Stars, in: Eggleton, P.P., Pringle, J.E. (Eds.), *Interacting Binaries*, p. 367. doi:doi:[10.1007/978-94-009-5337-6_14](https://doi.org/10.1007/978-94-009-5337-6_14).
- Warner, B., 1995. *Cataclysmic variable stars*. Cambridge University Press 28.
- Watson, C.L., Henden, A.A., Price, A., 2006. The International Variable Star Index (VSX). *Society for Astronomical Sciences Annual Symposium* 25, 47.
- Wei, L., Shengbang, Q., 2023. Investigation of Superhumps in SU UMa-type Dwarf Novae Based on the Observations of TESS. *ApJ* 954, 135. doi:doi:[10.3847/1538-4357/acebdf](https://doi.org/10.3847/1538-4357/acebdf), [arXiv:2405.11843](https://arxiv.org/abs/2405.11843).
- Whitehurst, R., 1988. Numerical simulations of accretion discs - I. Superhumps : a tidal phenomenon of accretion discs. *MNRAS* 232, 35–51. doi:doi:[10.1093/mnras/232.1.35](https://doi.org/10.1093/mnras/232.1.35).
- Whitehurst, R., King, A., 1991. Superhumps, resonances and accretion discs. *MNRAS* 249, 25–35. doi:doi:[10.1093/mnras/249.1.25](https://doi.org/10.1093/mnras/249.1.25).
- Wood, M.A., Still, M.D., Howell, S.B., Cannizzo, J.K., Smale, A.P., 2011. V344 Lyrae: A touchstone su uma cataclysmic variable in the kepler field. *ApJ* 741, 105. doi:doi:[10.1088/0004-637X/741/2/105](https://doi.org/10.1088/0004-637X/741/2/105).
- Wood, M.A., Thomas, D.M., Simpson, J.C., 2009. Sph simulations of negative (nodal) superhumps: a parametric study. *MNRAS* 398, 2110–2121. doi:doi:[10.1111/j.1365-2966.2009.15252.x](https://doi.org/10.1111/j.1365-2966.2009.15252.x).